Emissions of methylamines from cattle husbandry

Elisabeth Emilie Syse

Thesis submitted for the degree of
Master of Science in Chemistry
60 credits

Department of Chemistry
Faculty of Mathematics and Natural Sciences

UNIVERSITY OF OSLO

June 2021

Emissions of methylamines from cattle husbandry

2021

Emissions of methylamines from cattle husbandry

Author: Elisabeth Emilie Syse

http://www.duo.uio.no/

Printed at Reprosentralen, Universitetet i Oslo

Abstract

Gaseous amines play an important role in atmospheric chemistry, affecting both climate and human health. They act as precursors to particles and break down to form potentially toxic products. Cattle husbandry have been established as one of the predominant atmospheric sources of gaseous amines, yet little is known about the emission rates of amines in this sector. To increase the basic knowledge in this field, monomethylamine, dimethylamine, and trimethylamine emissions were monitored during winter in a cattle barn at the Livestock Production Research Center of the Norwegian University of Life Sciences at Ås over a period of 46 days using a state-of-the-art mass spectrometer. The aim of this study was to determine amine volume mixing ratios in air and to determine amine emission rates. Trimethylamine (22 ± 11 mg h^{-1} $animal^{-1}$) was found to be the most abundant methylamine emitted from the cattle barn, followed by monomethylamine (1.9 ± 0.9 mg h^{-1} $animals^{-1}$) and dimethylamine (0.49 ± 0.17 mg h^{-1} $animals^{-1}$). For comparison, the emission rate of ammonia was found to be 1.5 ± 0.6 g h^{-1} $animal^{-1}$. To the best of my knowledge, this was the first study to determine monomethylamine and dimethylamine emission rates from cattle husbandry. Diurnal profiles and statistical analyses of the three methylamines versus the temperature suggested a temperature dependence of emissions, which was most apparent for monomethylamine. High levels of correlation between the three methylamines and ammonia indicated common sources, animal excrements being the most prominent candidate. However, laboratory measurements suggested silage food as an additional, minor source of trimethylamine.

Preface

To the warm memories of my grandmother Else Syse and my aunt Siv Nordrum, who were taken away from us during the writing of this thesis.

Acknowledgments

First and foremost, I would like to thank my supervisor Armin Wisthaler for giving me an opportunity to work within the Atmospheric Chemistry Group at UiO and thus introducing me to such an exciting field. Your desire and ability to pursue new and interesting ideas, combined with your knowledge in atmospheric sciences, are truly inspiring. Thank you for having faith in my work and showing me just how creative science can be.

Second, a huge thank you to my co-supervisor, Alexander Håland, for the many hours spent on teaching me the PTR-MS method and several discussions concerning amines, politics, philosophy, etc. Thank you for always leaving the door open for me, even when you have plenty of work yourself. Your charisma, down-to-earth approach, and natural teaching abilities have been essential to my learning progress.

Thank you to our main contact person, Irma Caroline Oskam, and the whole staff at Livestock Production Research Center at Ås, without which the measurements campaign and thus the main project of my thesis would not have been possible.

A special thank you to Tomas Mikoviny, the senior engineer at the atmospheric group at UiO, for the many hours spent preparing and installing the mobile laboratory for the field measurements campaign, and for always helping with data processing and the general operation of the instrument. Thank you to the whole Atmospheric Chemistry Group for watching several hours of presentations regarding the field campaign for my master thesis, despite not being directly involved in the project.

A personal thank you to my favorite study mate and partner Markus Sørensen for helping me out with coding-issues and for being an emotional support during my master's. Finally, a warm thank you to my whole family for your endless love and support, and for being especially close during the tough months of March and April 2021.

Table of Contents

Abbreviations

ACR	Air change rate
DC	Direct current
DMA	Dimethylamine
DT	Drift tube
EA	Ethylamine
EI	Electron ionization
FC	Flow controller
GDT	Glass drift tube
HPLC	High performance liquid chromatography
LCU	Liquid calibration unit
LU	Livestock unit
MMA	Monomethylamine
MS	Mass spectrometry
PA	Proton affinity
PEEK	Polyether-ether-ketone
PFA	Perfluoroalkoxy-alkanes
PTR	Proton transfer reaction
RF	Radio frequency
RH	Relative humidity
SHF	Senter for Husdyrforsøk
TMA	Trimethylamine
ToF	Time-of-Flight
UiO	University of Oslo

1. Introduction and overview of the field

1.1 Amines in the atmosphere

Amines are a group of organic compounds that consist of a basic nitrogen atom with a lone pair of electrons, and up to three alkyl or aryl groups. They are derivatives of ammonia (NH_3) where one or more of the H-atoms have been substituted, and are divided into three subgroups: primary, secondary, and tertiary amines. A fourth group comprises the quaternary amines which differ from the other three subgroups in being a charged species, i.e., they are salts.

Amines are universal building blocks found in all living organisms: Nucleic acids are comprised of cyclic amines, and amino acids contain amine functional groups. With living organisms being ubiquitous on Earth, amino acids and amines are also expected to be found in the atmosphere. However, amino acids have low vapor pressures and are thus more prominent in the condensed phase in the atmosphere (Ge et al., 2011a). In contrast, low molecular weight amines have a high vapor pressure and readily partition to the gaseous state. Consequently, the most abundant atmospheric amines are low molecular weight alkylamines including monomethylamine (MMA), dimethylamine (DMA), and trimethylamine (TMA) (Fig. 1.1) (Ge et al., 2011a). In total, over 150 gaseous amines and 30 amino acids have been observed in the atmosphere (Ge et al., 2011a).

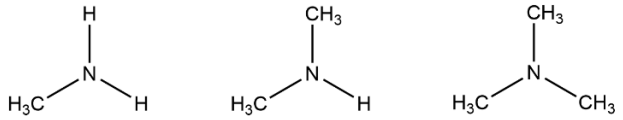

1. Monomethylamine Dimethylamine Trimethylamine

Figure 1.1: The chemical structures of MMA (left), DMA (middle), and TMA (right).

Gaseous amines are highly reactive in the atmosphere and are found almost exclusively in proximity to their emission source. The two most important reaction pathways of small alkylamines in the atmosphere include: i) oxidation reactions by hydroxyl (OH) or nitriate (NO_3) radicals to form amides, imines, and carcinogenic nitramines and nitrosamines and ii) reactions with acids to form ultrafine particles with potential effects on human health and the climate.

1.2 Atmospheric oxidation of amines

Gas-phase oxidation is the main sink for atmospheric amines. The daytime oxidation of the three methylamines primarily occurs through fast reactions with OH-radicals (Ge et al., 2011a; Schade & Crutzen, 1995; Yu & Luo, 2014). Oxidation by ozone (O_3) also occur, although slower and thus less effective (Ge et al., 2011a; Nielsen et al., 2012). OH-radicals are produced photolytically, which is why the OH-radical induced oxidation occurs during the day. Reaction-rate coefficients, k, display the speed of a chemical reaction, and for the three methylamines, k_{OH} is in the range between 2 – 7 x 10^{-11} cm^3 $molecule^{-1}$ s^{-1} (Nielsen et al., 2012). The OH-lifetimes of MMA, DMA and TMA are thus between 4 – 14 hours (Ge et al., 2011a; Nielsen et al., 2012). The atmospheric removal of NH_3 by OH-radicals is much slower, resulting in an OH-lifetime up to 73 days (Ge et al., 2011a; Yu & Luo, 2014). At night, the gas-phase oxidation of amines occurs through NO_3-radicals, with k_{NO3} being in the range of 1 – 5 x 10^{-13} cm^3 $molecules^{-1}$ s^{-1} (Nielsen et al., 2012).

The pathways for the OH-indices degradation of MMA, DMA, and TMA are presented in Fig. 1.2 – 1.4. Minor products (highlighted in red) are nitramines and nitrosamines, which are carcinogenic or potentially carcinogenic compounds, respectively. However, the formation of nitramines and nitrosamines is highly dependent on the availability of nitrogen species (NO_x = NO and NO_2) (Nielsen et al., 2012). Nitrosamines are rapidly degraded by sunlight, which makes the formation of nitramines a bigger health concern.

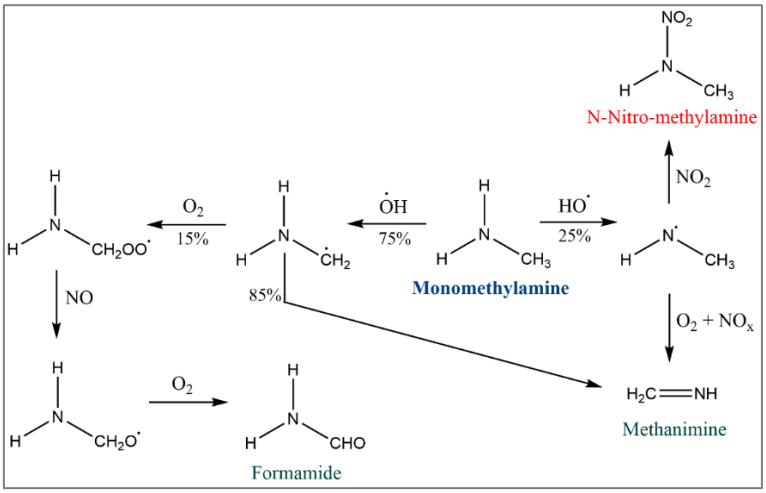

Figure 1.2: An outline of the oxidation of MMA initiated by OH-radicals. The major products are methanimine and formamide, while the harmful N-Nitro-methylamine is only a minor product, depending on atmospheric NO_2 concentrations. The scheme is adapted from Nielsen et al. 2012.

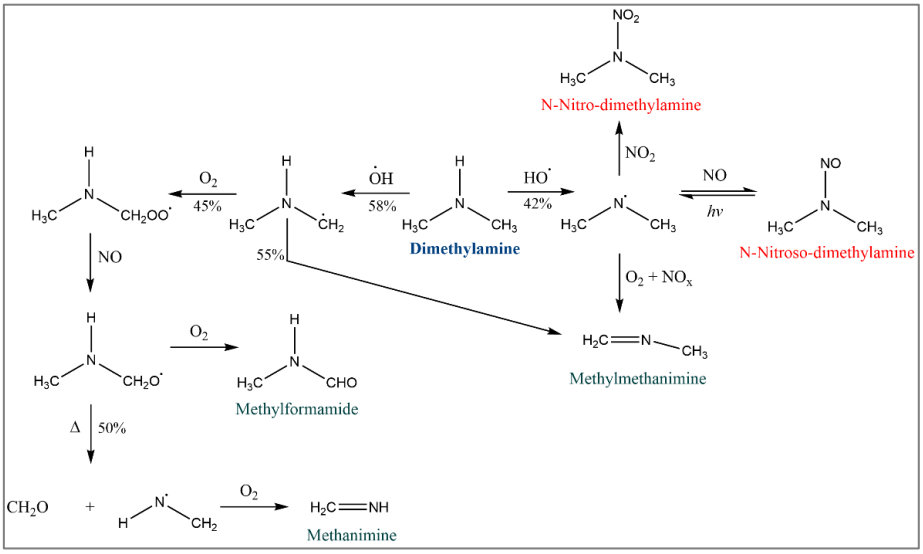

Figure 1.3: An outline the oxidation of DMA initiated by OH-radicals. The major products are methanimine, methylmethanimine and methylformamide, while the minor products N-Nitro-dimethylamine and N-Nitroso-dimethylamine are only formed in the presence of NO_x. The scheme is adapted from Nielsen et al. 2012.

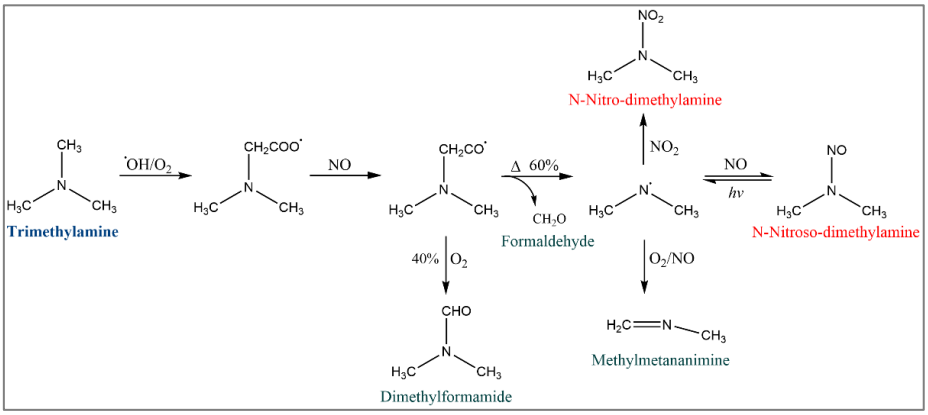

Figure 1.4: An outline of the oxidation of TMA initiated by OH-radicals. Major products are methylmetanimine, dimethylformamide and formaldehyde. N-Nitro-dimethylamine and N-Nitroso-dimethylamine are produced in small amounts, depending on the availability of NO_x. The scheme is adapted from Nielsen et al. 2012.

An important aspect of atmospheric amine oxidation is the potential formation of nitrous oxide (N_2O), which is a potent greenhouse gas. Schade & Crutzen (1995) presented possible production pathways of N_2O from the methylamines, which is based on photochemical breakdown of imines and amides. It was estimated that amine oxidation could contribute to a 6 – 10 % increase in the annual production of N_2O from animal husbandry. Thus, emissions of methylamines may also be problematic in the context of global warming.

1.3 Atmospheric acid-base reactions involving amines

Amines are basic compounds and are thus involved in acid-base reactions with gaseous acids in the atmosphere, the most prominent being nitric acid (HNO_3), sulfuric acid (H_2SO_4), and hydrogen chloride (HCl) (Ge et al., 2011a; Lee & Wexler, 2013). Volatile amines and acids react to form non-volatile aminium salts (Eq. 1.1 – 1.2), thereby forming atmospheric nanoparticles.

$$NR_3\ (g) + HX\ (g) \leftrightarrow HNR_3X\ (s) \qquad 1.1$$

$$NR_3\ (g) + H_2SO_4\ (g) \leftrightarrow (HNR_3)_2SO_4\ (s) \qquad 1.2$$

where NR_3 is either NH_3 or an amine, and HX is either HCl or HNO_3. Atmospheric HNO_3 concentrations are typically larger than HCl and H_2SO_4 (Ge et al., 2011a; Murphy et al., 2007). Thus, amines predominantly react with HNO_3 to form aminium nitrate particles.

Considering that atmospheric concentrations of NH_3 are typically several orders of magnitude larger than amines, it remains uncertain if amines can compete with NH_3 in atmospheric acid-base chemistry (Murphy et al., 2007). However, Ge et al. (2011a) reported that the particle formation by atmospheric reactions involving MMA and DMA accelerates at higher temperatures and becomes considerable (compared to particle formation induced by NH_3) over 20 °C. Furthermore, thermodynamic studies conducted by Ge et al. (2011b) indicate that at low temperatures, aminium salt particles are preferably formed relative to the ammonium salt. Almeida et al. (2013) found that DMA volume mixing ratios over ~3 parts-per-trillion (pptV) enhanced particle formation with sulfuric acid about three orders of magnitude relative to NH_3. These laboratory studies suggest that amines may play an important role in atmospheric particle formation. Confirming evidence from field measurements is, however, still scarce. Sorooshian et al. (2008) found high amine particle levels (14 – 23% of particulate ammonia) downwind of a large feedlot, indicating that amines and in particular amines from agriculture may contribute to particle formation in the atmosphere.

1.4 Agricultural emissions of amines to the atmosphere

Gaseous amines originate from both anthropogenic and natural sources. Natural sources of amines include emissions from the ocean, from biomass burning, and from vegetation. Anthropogenic sources include emissions from agriculture, combustion, tobacco smoke, and carbon capture plants utilizing amine technology.

Agriculture and animal husbandry are the main anthropogenic sources of amines to the atmosphere (Ge et al., 2011a; Murphy et al., 2007; Schade & Crutzen, 1995). According to Schade & Crutzen (1995) and Ge et al. (2011), cattle are the largest emitter of amines and NH_3 from animal husbandry. Typical ambient mixing ratios of NH_3 range from 0.1 to 1 ppbV, but may reach several ppmV in proximity to agricultural sites (Sorooshian et al., 2008). Gaseous amine concentrations from animal husbandry are typically 2 – 3 orders of magnitude lower than NH_3 concentrations (Ge et al., 2011a; Qiu & Zhang, 2013; Schade & Crutzen, 1995; Sintermann et al., 2014).

The production of NH_3 from cattle is well understood and has been described in several former studies, e.g., by Groot Koerkamp et al. (1998) and Ishler (2016). NH_3 is mainly formed via bacterial degradation of excremental nitrogen. The enzyme urease, which is produced by bacteria present in animal feces, catalyzes the hydrolysis of urea (1.3). Hence, the emissions of NH_3 from feces or urine itself is minimal.

$$\underset{\text{(urea)}}{CO(NH_2)_2\,(aq)} + H_2O\,(g) \xrightarrow{\text{urease}} CO_2\,(g) + NH_3\,(g) \qquad (2.3)$$

TMA accounts for almost 75% of the total gaseous amine emissions from animal husbandry, with feces, urine, and slurry (i.e., a mixture of the two) being the acknowledged, predominant sources (Groot Koerkamp et al., 1998; Schade & Crutzen, 1995; Sintermann et al., 2014). TMA is produced by microorganisms from dietary constituents in the rumen of the animals. It diffuses through the wall of the rumen into the bloodstream or forms other compounds such as methane (Fig. 1.5). TMA is also converted into a TMA-precursor, trimethylamine-N-oxide (TMAO), in the liver or kidney of ruminating animals, which is mainly emitted through urinary excretion.

The feces contain TMAO-transforming microbes, which produce TMA in the expelled excrements. TMA in excrements may be demethylated by aerobic microorganisms to form DMA, MMA, and finally NH_3.

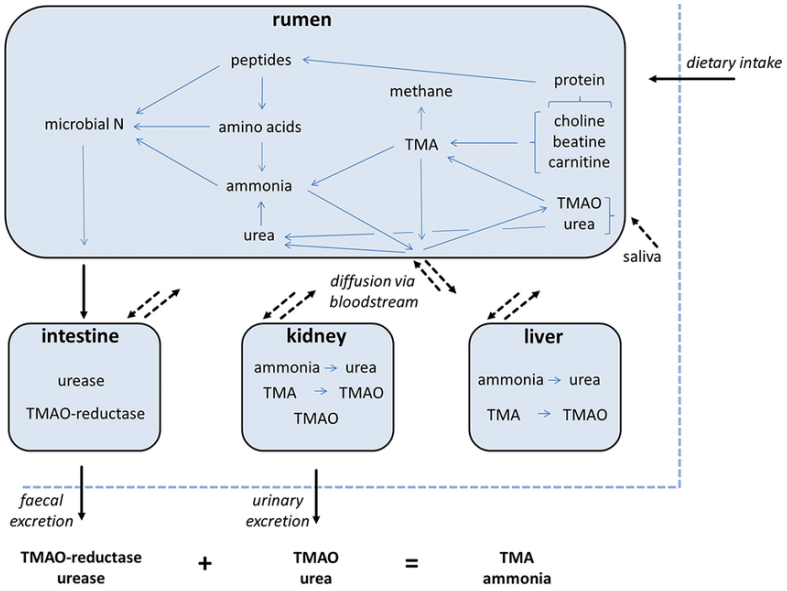

Figure 1.5: The biological production of TMA and NH_3 in ruminating animals, including cattle (Sintermann et al., 2014). This scheme was obtained from Sintermann et al. (2014).

Due to the high TMA content in rumen juice, Kuhn et al. (2011) suggested the breath of ruminating animals to be the dominating source of TMA from cattle, not animal excrements. However, most research on the subject have identified excreta as the main atmospheric source of TMA from animal husbandry (Ge et al., 2011a; Kammer et al., 2020; Schade & Crutzen, 1995). Furthermore, Sintermann et al. (2014) did not observe a correlation between methane and TMA emissions from cattle. Since methane is produced by rumination and emitted through the mouth of the ruminating animal, a correlation between the two compounds would be expected if TMA were predominantly emitted by rumination.

MMA and DMA have also been measured inside livestock buildings, with DMA mixing ratios being in the range of 2 – 10 times lower than MMA levels (Ge et al., 2011a; Schade & Crutzen, 1995). No previous work has characterized the production pathways of MMA or DMA from cattle. However, previous studies strongly suggest that MMA and DMA originate from the same sources as NH_3 and TMA and may be produced by similar pathways as TMA or produced by aerobic demethylation of TMA in animal excrements (Schade & Crutzen, 1995; Sintermann et al., 2014). Schade & Crutzen (1995) suggested that an additional minor source to MMA inside livestock buildings could be by decarboxylation of glycine (a non-essential amino acid).

Ge et al. (2011a) summarized the estimated global emissions (± standard deviations) of NH_3 and methylamines from cattle husbandry: ~17600 Gg N yr^{-1} for NH_3, 20 ± 11 Gg N yr^{-1} for MMA, 11 ± 7 Gg N yr^{-1} for DMA, and 94 ± 24 Gg N yr^{-1} for TMA. These quantities account for ~44% of the total global emissions of the methylamines, i.e., 125 ± 42 Gg N yr^{-1} of a total of 285 ± 78 Gg N yr^{-1} (Ge et al., 2011a). NH_3, MMA, DMA, and TMA emissions from cattle make up 86% of the total emissions from livestock, indicating that cattle are the main sources of amines in animal husbandry (Ge et al., 2011a). However, Kammer et al. (2020) recently found higher TMA emission rates in a sheep pen than in a dairy cattle barn. This indicates that more research on emission rates is needed for better characterizing amine emissions from animal husbandry.

1.5 Challenges with amine measurements

The main reason why atmospheric amines are poorly studied is the fact that they are difficult to measure. They are typically present at low atmospheric mixing ratios, i.e., in the pptV-range, implying that atmospheric amine analyzers must have low detection limits. In addition, amines have a high affinity to surfaces (Ge et al., 2011b), meaning that they are easily adsorbed onto filters, inlet lines or other instrumental surfaces. This may cause slow instrument response times and sample losses. The last decade has seen a huge progress in the development of chemical-analytical techniques for atmospheric measurements. This is particularly true for the development of online mass spectrometers (MS). While it is beyond the scope of this thesis to detail the analytical developments, it is worth noting that only very little work on agricultural amine emissions have been carried out with these innovative instruments (Kammer et al., 2020; Sintermann et al., 2014).

1.6 Aim the study

The aim of my Master's project was to study emissions of MMA, DMA, and TMA from animal husbandry and relate them to emissions of NH_3. The work was motivated by the development of a new online mass spectrometer for the measurement of amines in the Atmospheric Chemistry Group at UiO. A field measurements campaign was carried out at a large animal husbandry research facility, and my work focused on emissions from cattle, which have been identified as a strong source of amines in previous work. Volume mixing ratios of MMA, DMA, TMA, and NH_3 were monitored in real time over a period of several weeks to answer the scientific questions:

1. What are the volume mixing ratios of MMA, DMA, and TMA inside the cattle barn, how do they vary over time, and how do they compare to volume mixing ratios of NH_3?
2. What are the emission rates of MMA, DMA, and TMA, and how do they compare to the emissions rates of NH_3?
3. What are the main sources of MMA, DMA, and TMA inside the cattle barn, and do they originate from the same sources?

As detailed above, the release of amines into the atmosphere may lead to the formation of oxidative derivatives and particles that are harmful to the human health. A recent study by Domingo et al. (2021) indicates that an average of 17 900 annual deaths in the US is related to air pollution from the agricultural sector. Amine emissions from cattle could play an important role in this context, and my work is aimed at increasing the basic scientific knowledge in this field.

2. Method

2.1 Amine measurements by using the PTR-ToF-MS

The measurements of amines in this project were executed using a prototype Vocus Proton Transfer Reaction Quadrupole-interface Time-of-Flight Mass Spectrometer (Vocus PTR-Qi-ToF-MS) which was originally developed by Tofwerk AG, Switzerland (Tofwerk, 2021) but later modified by coupling it to an ion source developed by Ionicon Analytik. The PTR-ToF-MS technique is fast, sensitive, and well established for detecting organic trace gases at volume mixing ratios (VMRs) down to pptV-levels (Ellis & Mayhew, 2014; Zhu et al., 2018).

2.1.1 Basic principle of PTR-MS

In mass spectrometry, only ionized analytes can be detected. Thus, the technique is dependent on the method of ionization. PTR is a method of ionization wherein the generation of charged analytes is achieved through the reaction of H_3O^+- ions with neutral molecules (A) according to Eq. 2.1. H_3O^+-ions protonate most organic, atmospheric compounds, including the amines of interest, but none of the inorganic constituents of air (e.g., N_2 and O_2).

$$H_3O^+ (g) + A (g) \rightarrow AH^+ (g) + H_2O (g) \quad (2.1)$$

Collisions between H_3O^+-ions and analyte molecules occur in the drift tube (DT) (Fig. 2.1).

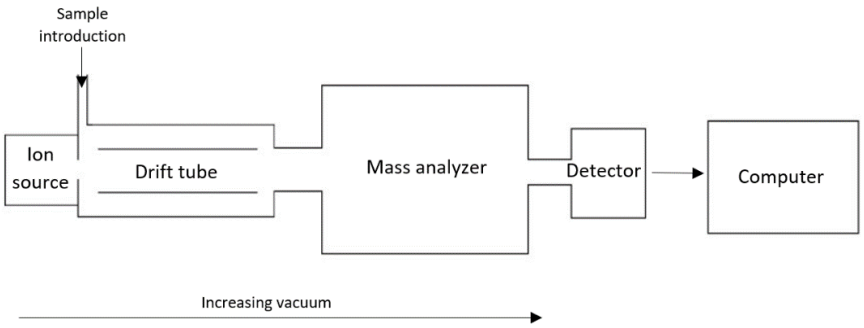

Figure 2.1: A general sketch of a PTR-MS-instrument. H_3O^+-ions are generated in the ion source and introduced to the DT together with a gaseous sample containing analyte molecules. Protonated analyte molecules are separated by a mass analyzer and detected by a detector.

The most important operational parameter is the ratio of the electric field strength (E) and the number density of neutral gaseous particles (N) in the DT (Eq. 2.2),

$$N = \frac{N_A}{V_M} * \frac{273.15}{T_{DT}} * \frac{P_{DT}}{101.325} \quad (2.2)$$

expressed as E/N where N_A = Avogadro's number ($6.022*10^{23}$), V_M = the molar volume of an ideal gas at 1 atm (22.414 m^3/mol), T_{DT} = temperature in the DT (K), and P_{DT} = pressure in the DT (kPa) (Ellis & Mayhew, 2014; Gross, 2017). Typical values range from 100-120 Td. Operating at higher E/N can cause excessive fragmentation of the analytes. Lower E/N can cause analytes to cluster with H_3O^+-ions, causing the formation of an adduct ion (e.g., $[A+H_3O]$). H_3O^+-ions can also cluster together with H_2O to form larger clusters, e.g., $(H_2O)H_3O^+$. Redundant formation of clusters can lead to a less efficient rate of analyte protonation and create more complicated spectra due to the increased number of clusters at higher masses.

The formation of protonated analytes is predicted by the proton affinity (PA) of H_2O, 165 kcal/mol, versus the PA of the analyte. Equation 2.3 displays the determination of the PA of analyte A in a gas phase reaction with a proton (H^+) at temperature T, determined by the enthalpy change of the reaction ($\Delta_f H°_T$) (Hunter & Lias, 2017):

$$PA\ (A) = \Delta_f H°_T\ (A) + \Delta_f H°_T\ (H^+) - \Delta_f H°_T\ (AH^+) \quad (2.3)$$

Only exothermic reactions, where the enthalpy change ($\Delta H°_T$) of the reaction between an analyte and H_2O is negative, generates protonated analytes. A reaction is exothermic when an analyte molecule has a *higher* PA than H_2O (Eq. 2.4) (Hunter & Lias, 2017).

$$\Delta H°_T = PA\ (H_2O) - PA\ (A) \quad (2.4)$$

2.1.1.1 Time-of-Flight mass analyzer

The PTS-MS-instrument in this assignment was combined with a ToF mass analyzer. In a ToF analyzer, protonated analytes are separated based on their flight time in a tube of known length. The time of flight (t) of an analyte is proportional to the square root of the *m/z*, the travel distance (d) and the ion velocity generated by a voltage (U) by the following relationship (Eq. 2.5) (Gross, 2017):

$$t = \frac{d}{\sqrt{2eU}}\sqrt{\frac{m}{z}} \quad (2.5)$$

where e = the elementary charge of a proton ($1.6*10^{-19}$ Coulomb). $\frac{d}{\sqrt{2eU}}$ is constant when the instrument is in use. When ions are introduced to a ToF mass analyzer they are exposed to an acceleration region where they gain momentum, before entering a field free region, absent of any electrical field (Ellis & Mayhew, 2014). Modern ToF analyzers are equipped with a reflectron to correct for a spread in the kinetic energy for identical ions as they enter the field free region (Fig. 2.2). In addition to this energy correction, it increases the ion travel distance which drastically improves the ion separation and thus the instrument resolving power (Gross, 2017).

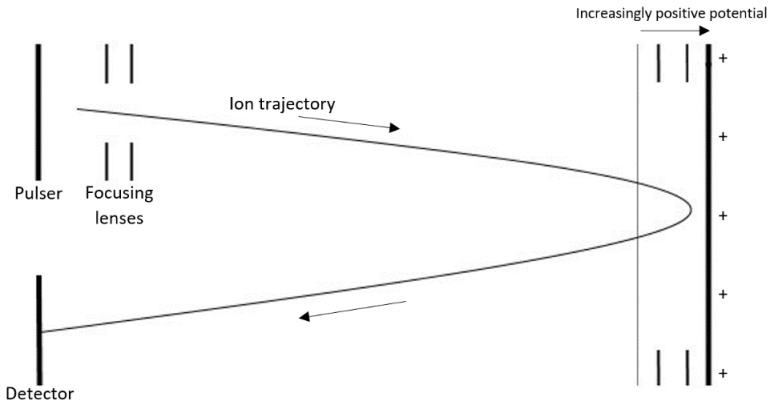

Figure 2.2: A sketch of the ToF mass analyzer with a reflectron. A pulser and two extractor electrodes (focusing lenses) make up the acceleration region of a ToF analyzer. By default, the voltages of the pulser and focusing lenses are identical until a rapid elevation of the pulser voltage is obtained, resulting in an ion being introduced to the field free region. The reflectron is made up of an increasingly positive potential, reversing the ion trajectory. Ions with a higher velocities penetrates the reflectron field deeper than ions at the same *m/z* traveling at a lower velocity, resulting in them reaching the detector at the same time.

The time intervals of ions separated by the ToF mass analyzer are in the nanosecond range. It is thus crucial to combine the ToF analyzer with a detector capable of responding to short time intervals between ions of different *m/z*. The microchannel plate (MCP) is designed to deliver a high time resolution (1 ns) and a high signal yield per ion (Ellis & Mayhew, 2014). Thus, the MCP is the detector of choice to combine with the ToF mass analyzer. The signal output from the MCP is recorded in ion counts per seconds (cps).

2.1.2 Instrument optimization for amine measurements

Several advancements were made to the PTR-MS-instrument applied in this thesis to develop a method optimal for amine measurements. The traditional DT made of stainless steel has been replaced with one constructed of glass (GDT). Both a traditional axial DC field and an RF field is generated along the drift tube. The DC potential is continuous and evenly distributed along the GDT, minimizing diffusion, scattering and thus wall loss of the ions inside the tube and instead focuses the ions into a narrow beam (Fig. 2.3).

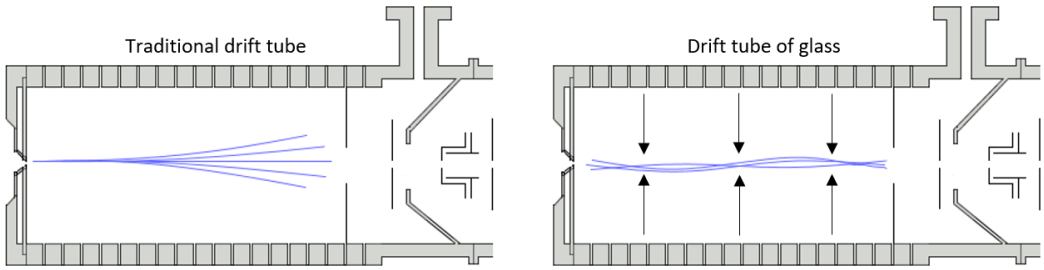

Figure 2.3: A comparison of a traditional drift tube (left) with the glass drift tube (right). The evenly distributed electric field in the glass drift tube secures a more effective ion focusing. The figure is made according to a depiction by Tofwerk (Tofwerk, 2021).

The overall effect of the GDT is increased sensitivity that allows for the detection of atmospheric trace gases at low ambient concentrations.

Three main steps were taken to reduce the amine adsorption to surfaces inside of the instrument:

1. An additional pump was coupled to the instruments inlet system to increase the inlet flow by a factor of 10-50, depending on previous configurations. With a higher inlet flow, sticky compounds have less dwell time in the inlet line and are therefore less prone to stick on to the inside surface of the inlet line.
2. The lines constructed of polyether-ether-ketone (PEEK) were replaced by perfluoroalkoxy-alkanes (PFA), a Teflon material. Advantages of replacing the lines with PFA were smoother, non-sticky, non-porous inner surfaces that prevent adsorption/absorption of most volatile organic compounds, high temperature tolerances (up to 260 °C), and strong dielectric resistance.
3. The PFA inlet line and the ion source were heated to 100°C to prevent condensation.

2.2 Field measurements at Livestock Production Research Center

The field measurement campaign was conducted in a cattle barn at Livestock Production Research Center (in Norwegian: “Senter for Husdyrforsøk”, abbreviated SHF) at Ås, located 40 minutes south of Oslo (Fig. 2.4). SHF is part of the Norwegian University of Life Sciences (NMBU) and conducts collaborative research on cattle, sheep, chickens, pigs, and goats, residing in separate barns (NMBU, 2021). The cattle residing in the barn where the measurements were carried out were Norwegian Red and Hereford cattle, not utilized for dairy production. The number of animals contained in the barn were kept constant at a total of 100 cattle throughout the campaign. The cattle barn was naturally ventilated with a total volume of 8105 m^3 (Figs. 6.1 – 6.2). The natural ventilation of the building was stimulated by fresh air entering through the main doors, one located at each end of the barn, spaces between the planks of the wooden walls and windows along the top of the roof. The main doors were normally closed during the winter to except for when tractors entered the barn.

Figure 2.4: A satellite image of SHF obtained from norgeskart.no. The cattle barn where the field measurements were conducted is marked in red.

The measurements set-up consisted of a mobile laboratory where the instrument was contained (Fig. 2.5). The trailer was installed outside, adjacent to the cattle barn where the measurements were conducted.

Figure 2.5: The mobile laboratory containing the instrument was positioned directly next to the cattle barn where the field measurements were carried out.

The field campaign lasted from 20.11.20 to 14.01.21, where data collected after 27.11.20 are presented in this assignment. During the first week of the campaign, between 20.11 – 25.11, instrument voltages and pressures were fine tuned. After the 26.11, no major changes were made to the instrument settings and set-up. The set-up for the calibrations was prepared on the 12.01.21, and field calibrations were conducted between 13.01 – 14.01.

2.2.1 Experimental set-up

A 15-meter heated line was extended from the inlet of the instrument to the inside of the barn for sampling of the air. The line was heated to 100°C and extended along the roof of the barn, with the inlet positioned approximately 5 meters above ground (Fig. 2.6).

Figure 2.6: An illustration of the inlet of the heated line. The inlet was installed close to the center of the roof of the barn. The windows along the roof contribute to the natural ventilation of the barn.

Fig. 2.7 illustrates the experimental set-up inside of the mobile laboratory:

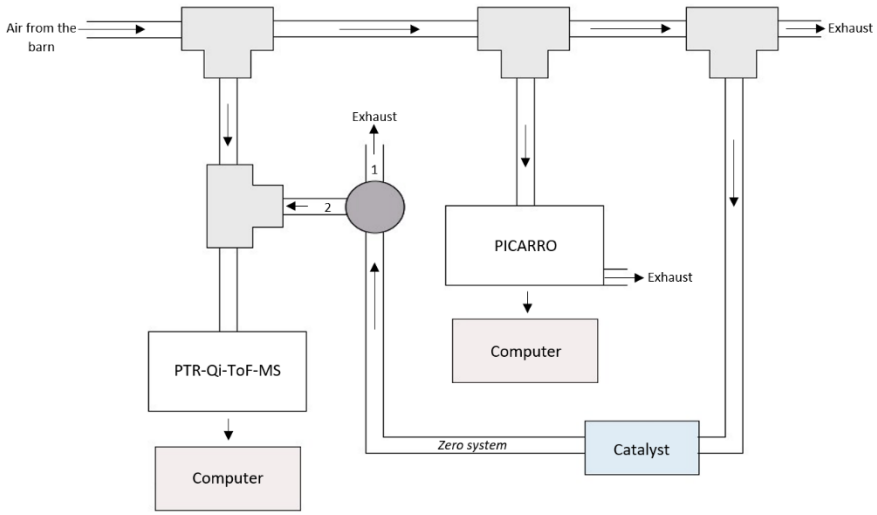

Figure 2.7: A simple sketch of the experimental set-up at SHF. Arrows mark the direction of the air flow. A total of 7 L/min was introduced from the cattle barn, where 0.5 L/min entered the PTR-MS-instrument, and 0.5 L/min entered the PICARRO. A valve regulating the activation of the zero system, providing the system with catalyzed air, was normally kept "closed" (position "1" in the figure was kept open, position "2" was kept closed), but was "opened" when the zero system was activated (position "2" was kept open, position "1" was kept closed).

A PICARRO instrument, rented from the Norwegian Institute for Air Research, was available for the measurements campaign between 26.11.20 – 04.01.21. The PICARRO provided quantitative CO_2 and CH_4 data (in ppmV) and was installed on the main inlet line (Fig. 2.7). Data from the PICARRO were available after 03.12.20.

A temperature/relative humidity sensor was installed 26.11.20 to record inside temperatures of the cattle barn. Temperature data was available after 10.12.20. The sensor was extended from the roof of the cattle barn, by the instrument inlet, to the computer inside of the mobile laboratory. By the end of December 2020, both outside and inside temperatures dropped below 5°C. The combination of low temperatures and a high humidity-level (~80%) lead to condensation inside the sensor that quickly froze. This caused the sensor to malfunction for most of the remaining campaign. Hence, temperature data was available between 10.12.20 – 30.12.20.

Instrument background was measured by flushing the instrument with cleaned air from a home-built catalyst daily between 01:00 to 02:30 (local time: UTC+1). Daily background measurements were subtracted from the data.

2.2.1.1 Instrument settings

The desired operating DT pressure of the instrument is 2.00 mbar. If the pressure gets much larger than 2.00 mbar, the rate of collisions in the DT would be less efficient (Ellis & Mayhew, 2014). Lower pressures result in electrical discharge inside the DT due to the increased E/N (Eq. 2.2). Discharge over time will not only disrupt the data but can also damage the drift tube and must be avoided. The drift tube pressure fluctuated between 1.90 – 2.08 mbar for the duration of the campaign. The drift tube voltage was 440 V, thus generating an E/N of 113 Td.

2.2.1.2 Set-up quality control: Leakage test

After the installment of the mobile laboratory at 20.11.20, a leakage test using methanol was performed on the instrument. During transport, the instrument was subjected to shaking and vibrations that could have resulted in parts becoming loose, thus creating leakage points in joints and connections. The procedure was to start the instrument and conditioning it until it was operational. Prior to the beginning of the measurements, a long cotton swab saturated with methanol was positioned next to junction points where leakages might have occurred. If there were leakages, a methanol spike would be observed in the mass spectrum. No peaks emerged in the mass spectrum from the leakage test.

2.2.2 Field calibrations

To quantify the raw signal output, thus converting it from cps into a VMR, the instrument sensitivity, hence the instrument response for a certain analyte, had to be determined. This is done by calibration of the analytes, thus by introducing solutions of known concentrations and creating a concentration gradient. By plotting the calibration, a sensitivity can be extracted from the slope of the calibration curve given in counts-per-second (cps), or more commonly, normalized cps (ncps) per VMR. The normalization is carried out to consider variations in the H_3O^+-ion count rate.

For the normalization process, the ^{18}O-isotope of the H_3O^+-ion and the ^{17}O-isotope of the $H_3O^+(H_2O)$-cluster, were applied (Eq. 2.6). For especially intense signals (~10^5 cps), the detector reaches its maximum output current causing the signal to be saturated, and no further output is provided by the detector for that specific *m/z* (Ellis & Mayhew, 2014). Due to a signal saturation of the more abundant ^{16}O-isotope of the H_3O^+-ion and the $H_3O^+(H_2O)$-cluster, the signals of the less abundant ^{17}O-isotopes were used for the data analysis. Factors of 476 for the ^{18}O-isotope of the H_3O^+-ion and 769 for the ^{17}O-isotope of the $H_3O^+(H_2O)$-cluster were multiplied with their respective cps to obtain signals corresponding to more abundant ^{16}O-isotope peak. The instrument generates H_3O^+-ions at a cps of ~10^6. Hence, this factor was multiplied with the ncps of the analyte to upscale the values relative to the magnitude of the H_3O^+-ion signal.

$$\mathrm{ncps} = \frac{[\mathrm{A}]_{\mathrm{cps}}}{([\mathrm{H_3O^+}]_{\mathrm{cps}}) * 476 + ([(\mathrm{H_2O})\mathrm{H_3O^+}]_{\mathrm{cps}}) * 769} * 10^6 \qquad (2.6)$$

Field calibrations were performed at the end of the field campaign at SHF. Two solutions were made for the calibrations: One with MMA, DMA, and TMA, and one with NH_3. The solutions were prepared one day prior to the calibrations. Detailed descriptions of the sample preparations are explained in the appendix (Eq. 6.1 – 6.7c).

A VMR gradient of 10, 8, 6 and 4 ppbV were recorded for MMA, DMA, and TMA, while a gradient of 12, 10, 7 and 5 ppmV was recorded for NH_3. A blank sample with HPLC-grade water was introduced for 30 minutes prior to the NH_3 calibration after a full night of flushing the system with HPLC-grade water, removing possible amine residues from the calibration unit.

2.2.2.1 Liquid calibration unit

The field calibrations of MMA, DMA, TMA and NH_3 were conducted using the IONICON liquid calibration unit (LCU). The LCU is designed for PTR-MS trace gas calibrations. The set-up ensures evaporation of the injected liquid solution by mixing it with a pressurized gas of synthetic air and introducing the mix into a heated evaporation chamber (Fig. 2.8) (IONICON, 2021). The evaporated sample is introduced to the PTR-MS-instrument by a line enclosed by a heated insulator which is coupled to the inlet of the instrument. The evaporation chamber and the line were heated to 100 °C.

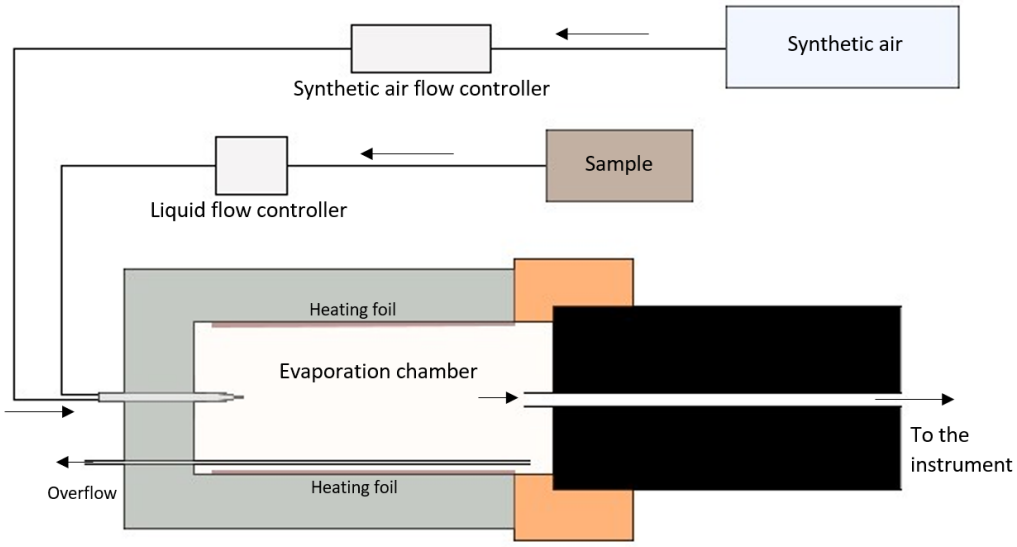

Figure 2.8: A simple sketch of the set-up of the LCU evaporation chamber, as depicted by IONICON. Arrows mark the direction of the flow.

The LCU liquid flow (µL/min) of the injected samples were adjusted to create a dilution gradient at a constant synthetic gas flow of 1 L/min. This eliminated the need of creating several calibration solutions at different concentrations.

2.2.2.2 Sensitivities of NH_3, MMA, DMA, and TMA

Calibration curves of NH_3, MMA, DMA, and TMA from the field calibration at SHF are presented in Fig. 2.9, where the slopes represent the sensitivities.

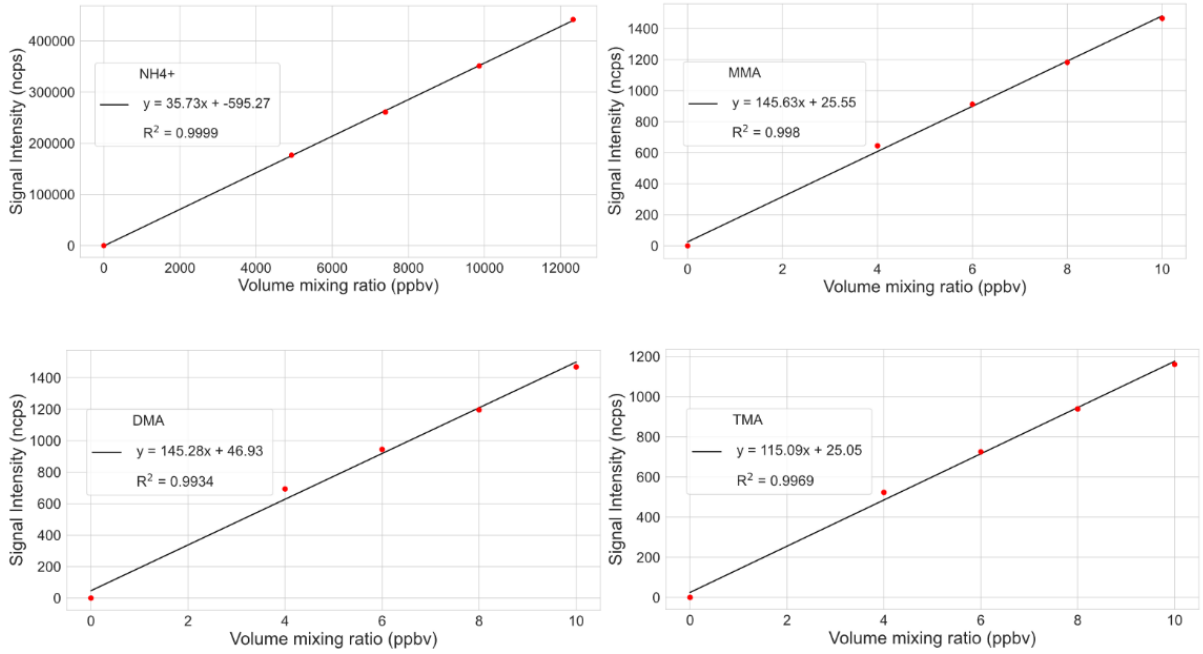

Figure 2.9: Calibration curves of NH_3 (upper left), MMA (upper right), DMA (lower left), and TMA (lower right) from the field calibrations at SHF.

Ideally, the instrument response is linear, as indicated by the R-squared (R^2) (Fig. 2.9). The R^2 is a statistical measure of correlation and linearity between variables in the data (between 0 and 1), where an R^2 of 1.00 corresponds to a "perfectly" linear response. as. By an R^2 of e.g., 0.50, 50 % of the data can be explained by the other variable in the regression analysis. The R^2 of the amine and ammonia calibrations were ~1.00, indicating a highly linear instrument response.

2.2.3 Calculation of emission rates

Emission rates for NH_3, MMA, DMA, and TMA were calculated by using the mass balance model described by Ngwabie et al. (2014) and Kammer et al. (2020) (Eq. 2.7).

$$E_i = Q * (C_{i,indoor} - C_{i,outdoor}) \quad (2.7)$$

where E_i is the emission rate (µg/h) for compound *i*, Q is the ventilation flow rate for the cattle barn (m^3/h), $C_{i,\,indoor}$ is the mean indoor concentration (µg or mg) for compound *i*, and $C_{i,\,outdoor}$ is the mean outdoor concentration (µg or mg) for compound *i*.

To calculate emission rates, the VMRs had to be converted into a unit of concentration (Eq. 2.8). Unlike VMRs, concentrations are dependent on atmospheric temperatures and pressures.

The standard temperature and pressure of 25°C and 1 atm, respectively, are commonly used for this conversion and were thus used in this thesis (Boguski, 2006).

$$C = \frac{p}{T} * VMR * MW \quad (2.8)$$

where C = concentration (mg/m^3), p = pressure (atm), T = temperature (°C), VMR = volume mixing ratio (ppmV), and MW = molecular weight (g/mol).

It was assumed that outside concentrations of NH_3 and the methylamines were much lower than inside concentrations, which is in accordance with the findings by Kammer et al. (2020). Thus, $C_{i,\,outside} = 0$ for NH_3 and the amines. The average emission rates were reported in g animal^{-1} h^{-1}.

The most common method for determining Q in naturally ventilated barns is by a CO_2 mass balance equation (Harper et al., 2009; Janke et al., 2020; Kammer et al., 2020; Ngwabie et al., 2014; Schmithausen et al., 2018). However, this method could not be applied to the measurements at SHF since the formula is based on the activity and heat production of *dairy* cattle. A suitable method was described by Laussmann et al. (2011), which was used to determine Q in the cattle barn at SHF. According to Laussmann et al. (2011), Q is calculated by multiplying the measured air change rate (ACR) or air changes per hour, λ (h^{-1}), with the room volume, V_R (m^3) (Eq. 2.9) (Laussmann & Helm, 2011). The floor plan of the cattle barn was provided by the administration at SHF, which was used to calculate the barn volume (Figs. 6.1 – 6.2).

$$Q = \lambda * V_R \quad (2.9)$$

2.2.3.1 Air change rate

The ACR can be derived at by applying a decay function to peaks in the spectrum (Laussmann & Helm, 2011). This method is named *the concentration decay function* (Eq. 2.10 – 2.10b).

$$C_j = C_0 * e^{-\lambda * \Delta t} \tag{2.10}$$

$$\ln C_j = \ln(C_0) - \lambda * (\Delta t) \tag{2.10a}$$

$$\lambda = \frac{[lnC_0 - lnC_j]}{(t_i - t_0)} \tag{2.10b}$$

where C_j = the concentration (here: in mg/m^3) at time *j*, and C_0 = the initial concentration. The decay function was applied to peaks triggered by an event (e.g., feeding or activation of the cleansing system), that manifested a gradual decay (Fig. 2.10).

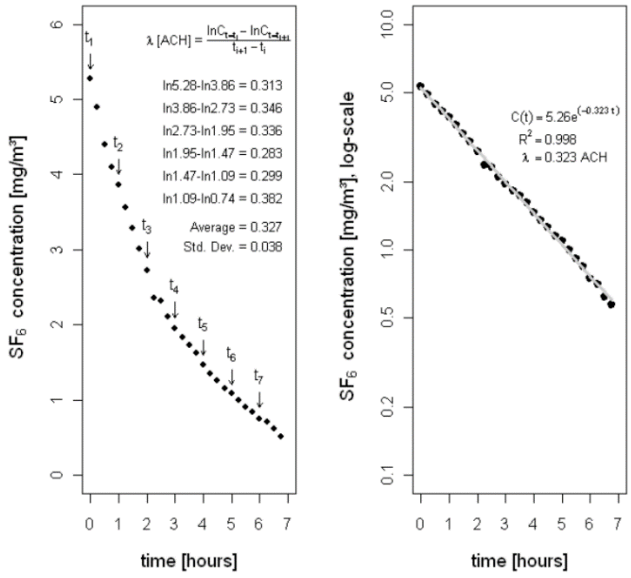

Figure 2.10: Decay curves after the emission of a tracer gas consisting of SF_6. The left figure illustrates the linear decay curve after 1 hour – 8 hours. The right figure illustrates the logarithmic decay curve of the same event. The figures are obtained from Laussmann et al. (2011).

In contrast to decay curves plotted in a linear scale, logarithmic decay curves are most often linear (Laussmann & Helm, 2011). Hence, linear regression were performed on logarithmic decay curves, and the slope from the regression represented the decay rate, thus the air changes per hour (Laussmann & Helm, 2011). Since the cattle barn was naturally ventilated, the ACR was anticipated to vary throughout the measurements campaign depending on outside wind conditions (Saha et al., 2013). Thus, daily ACR was extracted from the dataset, which were then used to determine daily emission rates.

Methanethiol displayed a low background and rapid decay curves after an event corresponding to Fig 2.10, indicating a low affinity to instrument surfaces (Fig. 6.3). Methanethiol was thus evaluated as suitable to determine the ACR of the cattle barn. However, methanethiol exhibited

periods in the mass spectrum absent of any activity, and individual ACRs for each day of the measurements campaign at SHF could thus not be determined. In total, 32 days were considered representative for the determination of ACRs, thus covering 70 % of the measurements campaign (Figs. 6.4 – 6.5).

2.3 Laboratory measurements at UiO

Prior to the field measurements at SHF, samples were collected from the cattle barn at SHF. Dynamic headspace measurements were conducted on the samples with the PTR-MS-instrument as a supplementary study to investigate possible sources of amines in the cattle barn. The samples were collected at the 01.10.20. The laboratory measurements were carried out between 02.10.20 – 04.10.20.

2.3.1 Samples from a cattle barn at SHF

The samples were collected from i) silage food (fermented and processed hay eaten by cattle), ii) manure collected from the floor of the barn, iii) feces sampled directly from the rectum of a cow, iv) food pellets, and v) sawdust. The samples were obtained in glass bottles of 100 mL and 50 mL (Fig. 6.6) and stored in room temperature. The manure collected from the floor of the barn is denoted as "Manure" and is believed to contain a mixture of feces and urine. Feces sampled from the rectum of a cow is denoted as "Feces" and contained no urine. The samples containing silage foods, manure and feces were considered to break down rapidly, and laboratory measurements on these samples were thus conduced the day subsequent to being sampled.

2.3.1.1 Experimental set-up

Fig. 2.11 is a configuration of the measurements set-up for the dynamic headspace measurements:

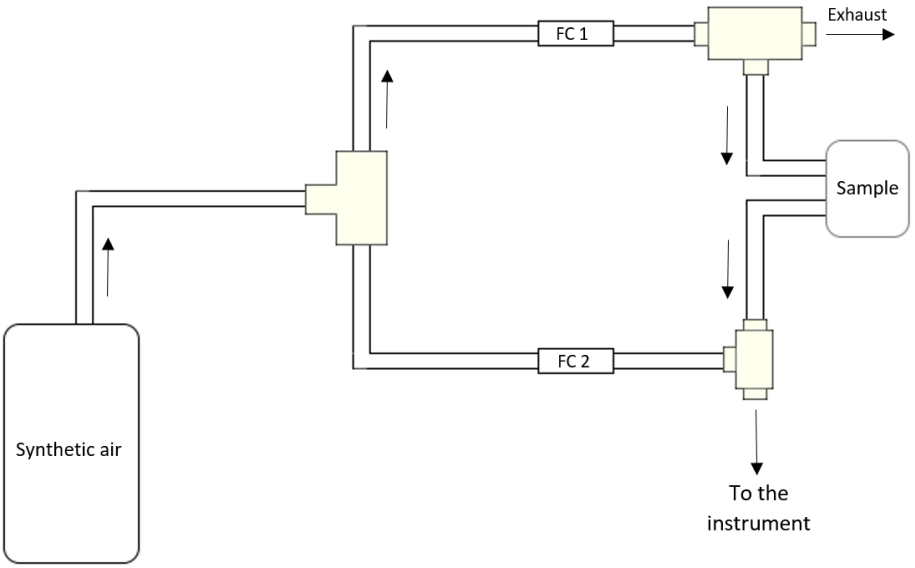

Figure 2.11: A description of the experimental set-up for the headspace measurements of the samples from SHF. A synthetic air gas flow of 1 L/min was mixed with the sample. Arrows mark the main air flow direction. The sample container had one air inlet and one air outlet, and the glass bottles containing the samples were directly placed without lid on in the container. FC 1 was set to 0.6 L/min to accommodate the volume of ~0.5 L/min entering the instrument. FC 2 was installed to dilute the sampling air in case of signal saturation in the mass spectrum.

2.3.1.2 Measurements protocol

Table 2.2 summarizes the measurements protocol of the samples. A zero measurement of synthetic air flushing the empty sample container was recorded for 30 minutes between every sample and prior to the measurements. In case of solidification, manure samples were gently blended with a glass stirrer immediately prior to the measurements.

Table 2.2: The measurements protocol for the laboratory measurements at UiO. To accommodate a signal saturation in the mass spectrum for the sample containing silage, a dilution flow was applied. No dilution flow was applied for the samples containing manure, food pellets or sawdust.

Sample	FC 1 synthetic air flow (L/min)	FC 2 synthetic air flow (L/min)	Measurement protocol at final flow (date)

Silage	0.3	0.2	02.10.20 13:15 – 14:25
Manure	0.6	0	02.10.20 15:35 – 16:50
Feces	0.6	0	02.10.20 17:45 – 19:10
Food pellets	0.6	0	04.10.20 14:30 – 15:35
Sawdust	0.6	0	04.10.20 16:05 – 17:10

2.4 Data processing

The raw measurement files were first processed in the IONICON PTR-MS Viewer (version 3.2.14) before statistical analyses and plotting were carried out in Jupyter Notebook running Python (version 3.9.1). The statistical analyses were performed to understand the level of correlation between NH_3, MMA, DMA, and TMA. This level of correlation was asserted by linear regression where the slope represents the relative abundances between the variables and the R^2-statistics represents the linear correlation. For the statistical analysis between the temperature and NH_3, MMA, DMA, and TMA, an exponential fit was found more suitable.

2.4.1 Peak integration

To quantify the raw data, the total cps of a peak in the mass spectrum must be known. This is achieved by peak integration, thus summing up the cps of one peak. Many peaks are part of a double or multiple peak(s) and must be separated manually by the software operator. Peak separation is highly dependent on the instrument resolution ($m/\Delta m$), thus the ability to distinguish two or more peaks in the spectrum. The resolution was 3500, which is high enough to separate isobaric compounds at the same nominal (integers) *m/z*, but may cause problems for ions at almost the same exact *m/z*.

If a peak is very intense, this may cause interferences for peak integration of adjacent peaks due to an elevated baseline. Typical *m/z* interferences of MMA, DMA and TMA peaks are O_2^+, NO_2^+ and the acetone ^{13}C-isotope, respectively. Proven to be a particularly difficult contaminant for amine analysis, creating intense signals in the mass spectrum, is the O_2^+ interference at exact *m/z* 31.989. O_2^+ is created in excessive amounts in the drift tube as sampling air is introduced. The O_2^+ peak is often so intense that MMA at exact *m/z* 32.049 is overshadowed and thus not integrated properly by the software (Fig. 6.7). This problem is not as prominent for DMA and TMA, as the NO_2^+ and acetone ^{13}C-isotope peaks are better separated from DMA and TMA, and their respective signal are usually not as intense as O_2^+. Thus, the base line for DMA and TMA are not affected the same way MMA is.

2.4.2 Compound assignment

Due to the presence of isotopes, fragments, and the fact that isobaric compounds cannot be separated in the mass spectrum, there are often some uncertainties related to the compound assignment in MS. The compound assignment in this thesis was based on mass accuracies, isotopic patterns, molecular formula suggestions by the software (a built-in module in the PTR-Viewer), fragments, and findings from earlier studies (Ge et al., 2011a; Kammer et al., 2020; Murphy et al., 2007; Ngwabie et al., 2014; Nielsen et al., 2012; Sintermann et al., 2014). The mass accuracy describes the difference between the accurate *m/z*, thus the experimentally determined *m/z*, and the exact *m/z*, thus the calculated and theoretical *m/z*, and is reported as a relative mass accuracy (ppm) (Eq. 2.11). Mass accuracies under 10 ppm are generally acknowledged as adequately low.

$$\text{Relative mass accuracy (ppm)} = \frac{(m/z_{\text{accurate}} - m/z_{\text{exact}})}{m/z_{\text{exact}}} * 10^6 \qquad (2.11)$$

2.4.2.1 The assignment of MMA, DMA, and TMA

Compounds assigned by the PTR-Viewer to the peaks at accurate *m/z* 32.050, 46.065, and 60.081 in the mass spectrum were $CH_3NH_2H^+$ (protonated MMA), $C_2H_6NHH^+$ (protonated DMA), and $C_3H_9NH^+$ (protonated TMA), respectively.

DMA has an isomer, ethylamine (EA), which was not possible to separate from DMA at accurate *m/z* 46.065 in the mass spectrum. However, Schade & Crutzen (1995) concluded that the relative concentrations of EA were significantly smaller than DMA in a cattle barn, and that only occasional traces of EA was observed. Except for Schade & Crutzen (1995), no research articles on EA from cattle were obtained for this thesis, and it was thus assumed that the peak at exact *m/z* 46.065 mostly consisted of DMA.

TMA has three isomers which may have contributed to the signal at accurate *m/z* 60.081 in the mass spectrum: n-propylamine, isopropylamine, and methylethylamine. Schade & Crutzen (1995) reported that the occurrences of n-propylamine and isopropylamine in cattle barns were insignificant compared to TMA. Furthermore, Ge et al. (2011) presented that methylethylamine is not a known emitter from agriculture, but from tobacco smoke. Hence, it was assumed that n-propylamine, isopropyamine, and methylethylamine were not significant contributors to the peak at accurate *m/z* 60.081.

2.4.2.2 The assignment of NH_3

Protonated NH_3 was assigned by the software to the peak at accurate *m/z* 18.034. The signal intensity of protonated NH_3 at exact *m/z* 18.033, was suspected to be above threshold for saturation of the detector due to high VMRs inside the cattle barn. However, this was disproven by examining the relationship between the peak of protonated NH_3 at accurate *m/z* 18.034 and the less intense signal of *ionized* NH_3, NH_3^+, at accurate *m/z* 17.025, asserted by a linear regression fit between the raw signals (Fig. 6.8). If the signal at accurate *m/z* 18.034 was saturated, the detector would not correctly recognize signal fluctuations, and the linear regression fit would deviate from linearity, which was not the case ($R^2 = 0.78$).

2.4.2.3 Mass accuracies

The mass accuracies of NH_3, MMA, DMA, TMA, the H_3O^+-ion, and the $H_3O^+(H_2O)$-cluster from the field measurements campaign at SHF, are presented in Table 2.3.

Table 2.3: The accurate *m/z* (experimentally determined *m/z*), exact *m/z* (theoretical *m/z*), and relative mass accuracy (ppm) of NH_3, MMA, DMA, TMA, the ^{18}O-isotope of the H_3O^+-ion, and the ^{17}O-isotope of the $(H_2O)H_3O^+$-cluster.

Compound	Accurate protonated *m/z*	Exact protonated *m/z*	Relative mass accuracy (ppm)
NH_3	18.03358	18.03383	-14
H_3O^+-isotope	21.02166	21.02209	-21
MMA	32.04952	32.04948	1.3
$(H_2O)H_3O^+$-isotope	38.03375	38.03351	6.4
DMA	46.06474	46.06513	-8.5
TMA	60.08050	60.08078	-4.7

The mass accuracies of the methylamines and NH_3 in Table 2.3 are mainly negative, indicating a shift in the spectrum towards lower accurate *m/z* compared to the exact *m/z*. However, the relative mass accuracies are generally low, thus increasing the confidence of accurately assigning the correct compound to an observed peak.

Based on the information above, NH_3, MMA, DMA, and TMA were assigned to the peaks presented in Table 2.3 and were thus concluded to be successfully observed in the cattle barn at SHF.

2.4.3 Stability of the primary ion signal

The stability of the H_3O^+-ion signal is important to consider in PTR-MS, as an unstable signal can dramatically affect the signal of the analytes (Ellis & Mayhew, 2014). The H_3O^+-ion signal remained stable through the measurements period, as presented in Fig. 2.12. Thus, variations in the analytes could not be explained by an unstable primary ion source.

Figure 2.12: The H_3O^+-ion signal (cps) (30-second moving average) from the field measurements campaign.

3. Results and discussion

3.1 Field measurements in the cattle barn at SHF

3.1.1 Time series of NH_3 and the methylamines and statistical analysis

Fig. 3.1 shows the time series of NH3, MMA, DMA, and TMA measured in the air inside the cattle barn at SHF during the 46-day measurement period. The data are reported as VMRs in ppmV (10^{-6} v/v) and ppbV (10^{-9} v/v).

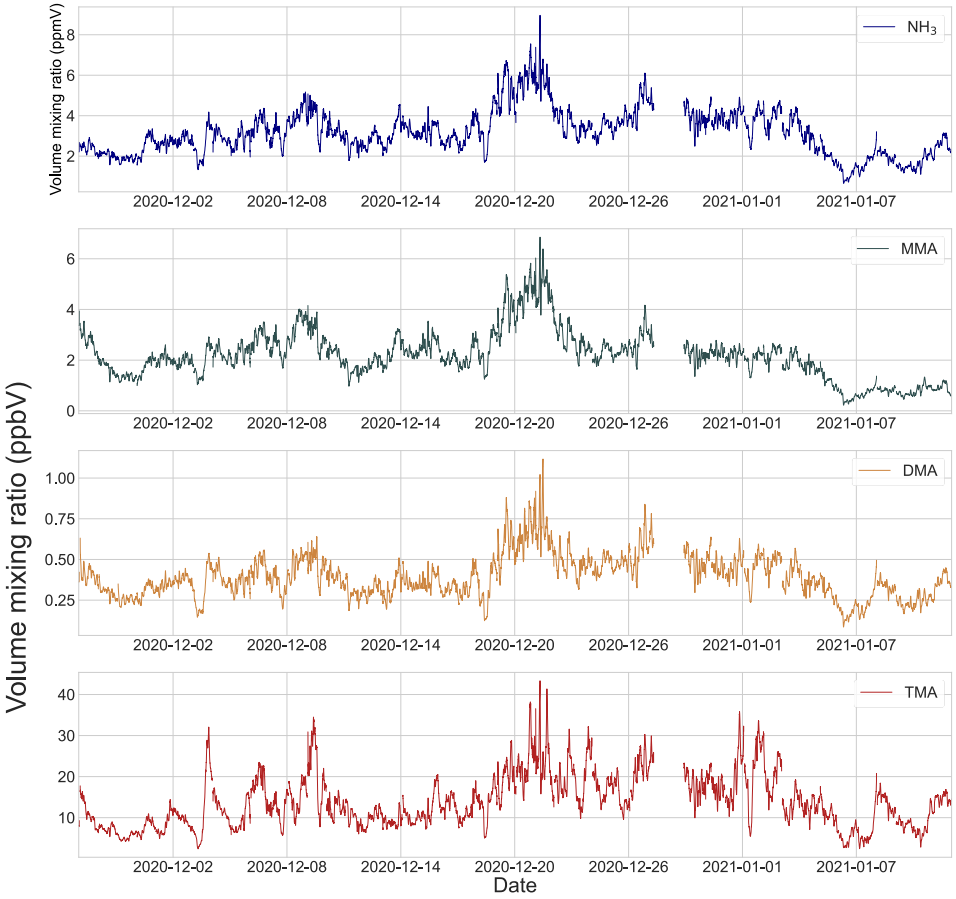

Figure 3.1: Time series (1-h moving average) of NH_3 (ppmV), MMA (ppbV), DMA (ppbV), and TMA (ppbV) as measured in the air inside the cattle barn at SHF. Short data gaps are instrument-zeroing periods; the data gap in the period 27.12 – 28.12. was caused by an instrument malfunction.

A statistical overview of the measured VMRs and concentrations is provided in Table 3.1.

Table 3.1: Mean (± std. deviation), median, and maximum VMRs and concentrations of NH_3, MMA, DMA, and TMA as measured in the air inside the cattle barn at SHF.

Compound	Unit	Mean ± Std. Dev.	Median	Maximum
NH_3	ppmV	3.2 ± 1.2	4.7	11.0
	mg m^{-3}	2.3 ± 0.8	3.4	8.0
MMA	ppbV	2.2 ± 1.0	3.9	8.8
	µg m^{-3}	2.8 ± 1.3	5.0	11.0
DMA	ppbV	0.39 ± 0.14	0.60	1.4
	µg m^{-3}	0.72 ± 0.25	1.1	2.6
TMA	ppbV	14 ± 6.7	20	61
	µg m^{-3}	33 ±16	49	147

The mean VMR of NH_3 measured in the air in the cattle barn was 3.2 ± 1.2 ppmV; the median VMR of NH_3 was 4.7 ppmV. These levels are similar to what has been reported in the literature. Ngwabie et al. (2014) reported an average NH_3 VMR of 3.8 ± 2.1 ppmV inside a dairy barn. Harper et al. (2009) reported average NH_3 VMRs ranging from <1 ppm to 5 ppm during wintertime. Finally, Kammer et al. (2020) reported average NH_3 VMRs between 2 and 4 ppmV.

TMA was the most abundant methylamine in the air in the cattle barn, with a mean VMR of 14 ± 6.7 ppbV and a median VMR of 20 ppbV. The maximum TMA VMR of 61 ppbV was recorded on the 21.12.2020. TMA was also the most abundant amine found in previous work by Sintermann et al. (2014) and Kammer et al. (2020). The latter reported average TMA VMRs between 5 and 10 ppbV in a dairy barn, which is slightly lower than the levels found in this study. However, the value given by Kammer et al. (2020) is based on a measurement period of only four days. Ge et al. (2011a) reported TMA concentrations inside livestock buildings ranging from 2 to 15 µg m^{-3}, which is significantly lower than the concentrations found in this study.

The mean VMR of MMA measured in the air in the cattle barn was 2.2 ± 1.0 ppbV; the median VMR of MMA was 3.9 ppbV. Kammer et al. (2020) did not report MMA, probably because of difficulties in measuring MMA with their PTR-MS instrument (see section 2.4.1). Ge et al.

(2011a) reported MMA concentrations inside livestock buildings in the range from 0.5 to 5.3 µg m^{-3}, which is similar to the levels found in this study.

The mean VMR of DMA measured in the air in the cattle barn was 0.39 ± 0.14 ppbV; the median VMR of DMA was 0.60 ppbV. No literature values were found for comparison.

The average diurnal profiles of MMA, DMA, TMA, NH_3, and air temperature inside the cattle barn are presented in Fig. 3.2.

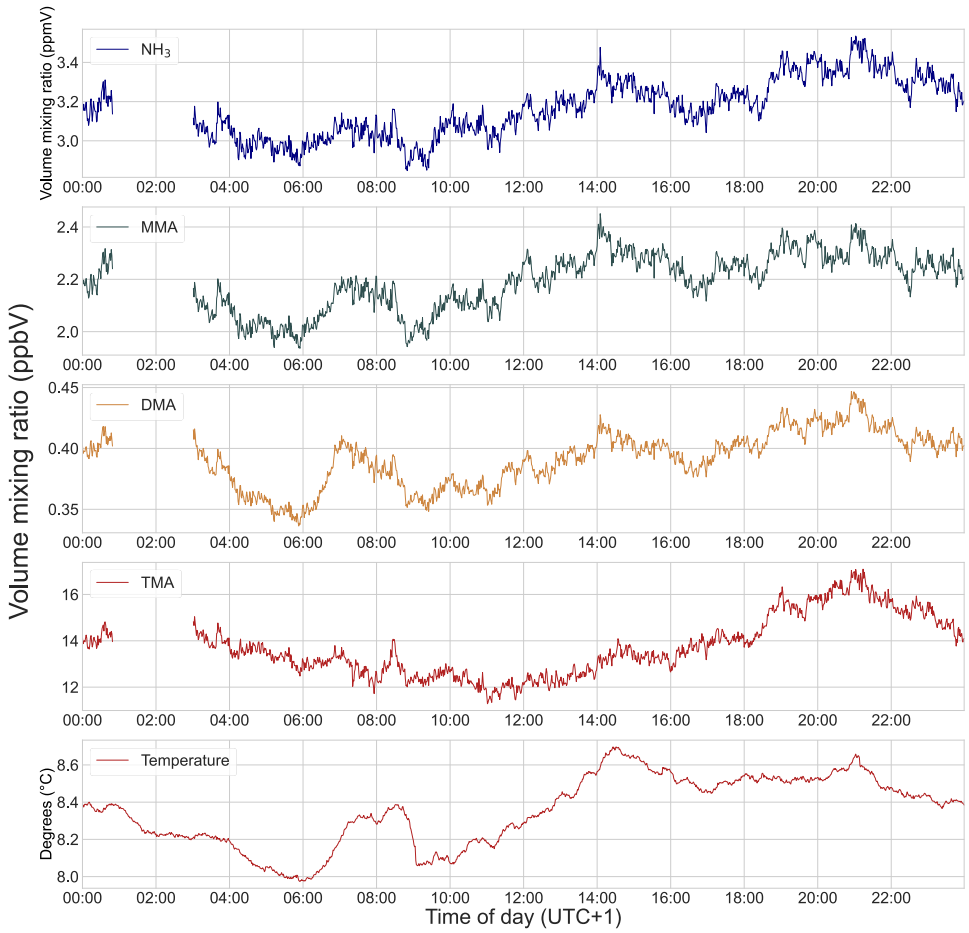

Figure 3.2: Mean diurnal profiles of NH_3 (ppmV), MMA (ppbV), DMA (ppbV), TMA (ppbV), and air temperature (°C) as measured inside the cattle barn at SHF. The presented data are 1-minute averages of the data collected between 27.11.2020 – 11.01.2021. The data gap between 01:00 and 02:30 is the instrument-zeroing period.

Variations in the mean diurnal profile were small; deviations from the day's average were only on the order of ±10%. Minimum NH_3, MMA and DMA VMRs were recorded during the early morning hours, while maxima occurred in the evening at around 21:00 local time. The average diurnal profiles of NH_3, MMA and DMA closely resemble the average diurnal profile of air

temperature inside the barn. TMA exhibited a slightly different diurnal pattern, with minimum VMRs occurring around noontime and maximum VMRs being recorded at around 21:00.

3.1.2 Relative abundances of MMA, DMA, and TMA

Fig. 3.3 shows scatter plots of MMA, DMA, and TMA, respectively, versus NH_3. MMA and DMA were highly correlated with NH_3, with R^2-values of 0.82 and 0.85, respectively. While correlations need to be interpreted with caution, this finding can be taken as a first evidence that MMA and DMA are formed and volatilized through the same or similar processes as NH_3. As outlined in the Introduction, NH_3 is mainly formed via bacterial degradation of excremental nitrogen. In the case of TMA, the correlation is lower (R^2 = 0.64) indicating some differences in the formation and/or volatilization of TMA and NH_3. This correlation was even lower for Sintermann et al. (2014), who reported an R^2 of ~0.43 between TMA and NH_3.

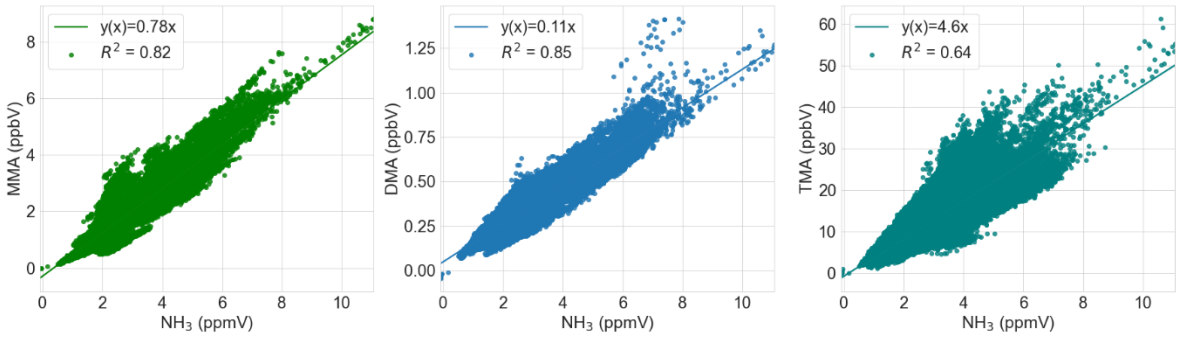

Figure 3.3: Scatter plots of MMA, DMA, and TMA, respectively, versus NH_3.

The abundances of MMA, DMA, and TMA relative to NH_3 were 0.78 x 10^{-3}, 0.11 x 10^{-3} and 4.6 x 10^{-3}, respectively. These values are in good agreement with the MMA:NH_3, DMA: NH_3, and TMA: NH_3 molar emission ratios reported by Schade & Crutzen (1995), which are 1.12 x 10^{-3}, 0.63 x 10^{-3} and 5.39 x 10^{-3}, respectively. A discrepancy exists for DMA, where the emissions in this study are lower than what is reported by Schade & Crutzen (1995). The TMA:NH_3 molar emission ratio reported by Sintermann et al. (2014) is between 0.5 – 1.5 % thus higher than the obtained ratio in this thesis.

3.1.3 TMA correlation with CH_4

As stated in the Introduction, Kuhn et al. (2011) suggested rumination as the dominating source of TMA from cattle. Fig. 3.4 shows that there is no linear correlation between TMA and CH_4 in the barn (R^2 = 0.04). This confirms the findings by Sintermann et al. (2014) where no correlation between TMA and CH_4 was obtained. Rumination is thus most likely not a source of TMA in the barn.

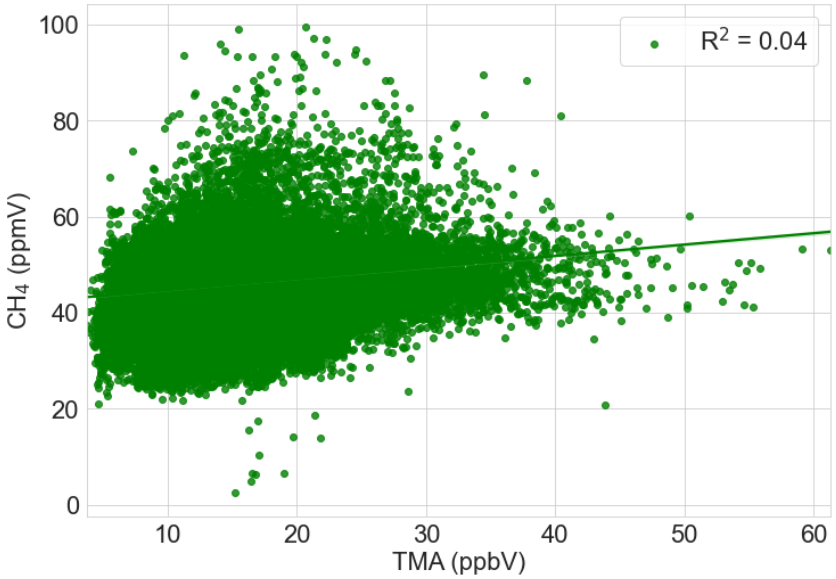

Figure 3.4: Scatter plot of TMA versus CH_4.

3.1.4 Temperature dependence of NH_3, MMA, DMA, and TMA VMRs

The average diurnal profiles shown in Fig. 3.2 have indicated that the VMRs of NH_3 and methylamines exhibit a temperature dependence. Fig. 3.5 shows the VMRs of NH_3, MMA, DMA, and TMA exponentially increasing with air temperature in the barn. The increase is seemingly strongest for MMA, followed by NH_3 and DMA. In the case of TMA, the temperature dependence is less obvious, but there still appears to be an underlying trend of VMRs increasing with temperature. It is not clear if the observed increase in the VMRs of NH_3 and methylamines is driven by increased formation rates (e.g., by increased bacterial activity) or by increased volatilization of NH_3 and the methylamines.

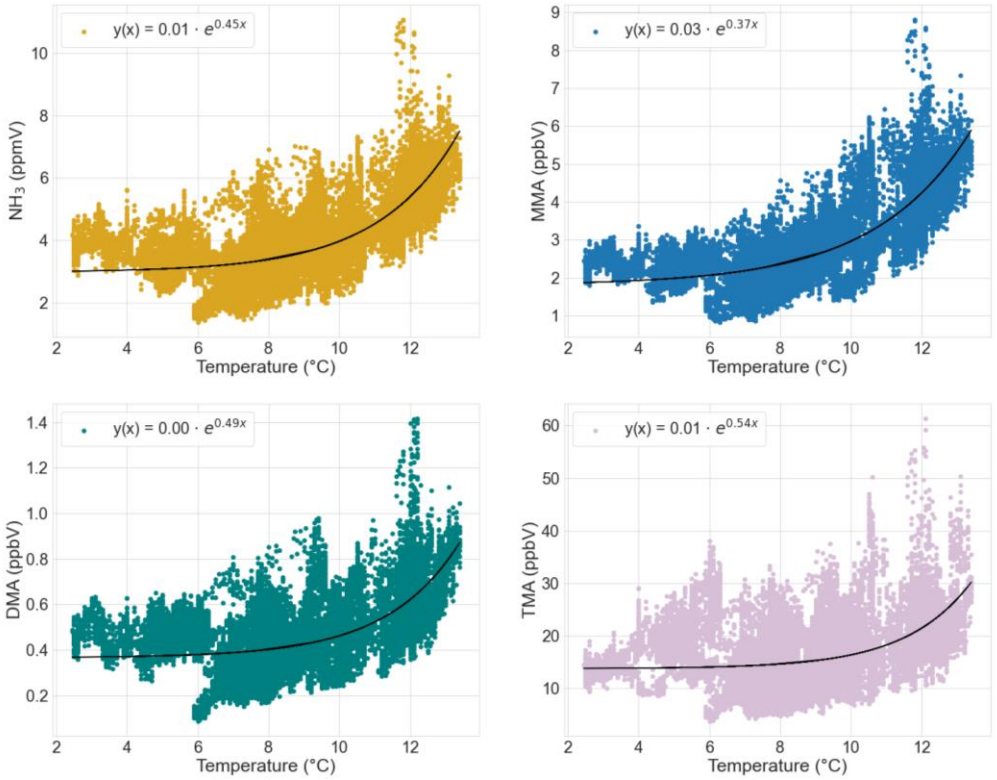

Figure 3.5: VMRs of NH_3, MMA, DMA, and TMA plotted as a function of air temperature in the barn.

3.1.5 Emission rates of NH_3, MMA, DMA, and TMA

Table 3.2 lists the measured ACRs in the naturally ventilated barn along with the emission rates (g h^{-1} $animal^{-1}$) of NH_3, MMA, DMA, and TMA, which were derived from the concentrations measured in the barn.

The daily ACRs measured were in the range between 2.7 and 14.0 h^{-1} and the mean ACR over the entire measurements campaign was 8.4 (± 3.2) h^{-1}. This results in a mean ventilation rate (Q) of 673 m^3 $animal^{-1}$ h^{-1}, which is within the typical range found for naturally ventilated barns during the wintertime/spring (Janke et al., 2020; Kammer et al., 2020; Ngwabie et al., 2009; Ngwabie et al., 2014).

Table 3.2: ACR (h^{-1}) and emission rates (g $animal^{-1}$ h^1) of NH_3, MMA, DMA, and TMA as measured day by day in the cattle barn.

Date	ACR	NH_3	MMA	DMA	TMA
	h^{-1}	g h^{-1} $animal^{-1}$	g h^{-1} $animal^{-1}$	g h^{-1} $animal^{-1}$	g h^{-1} $animal^{-1}$

2020-11-27	3.5	0.49	$9.6x10^{-4}$	$2.0x10^{-4}$	$7.1x10^{-3}$
2020-11-30	3.8	0.56	$6.5x10^{-4}$	$1.6x10^{-4}$	$5.5x10^{-3}$
2020-12-01	8.5	1.3	$1.7x10^{-3}$	$4.1x10^{-4}$	0.013
2020-12-02	9.2	1.5	$1.8x10^{-3}$	$5.0x10^{-4}$	0.016
2020-12-03	2.7	0.39	$5.0x10^{-4}$	$1.2x10^{-4}$	$6.5x10^{-3}$
2020-12-06	8.0	1.7	$2.3x10^{-3}$	$5.2x10^{-4}$	0.027
2020-12-07	11	1.9	$2.6x10^{-3}$	$5.1x10^{-4}$	0.023
2020-12-08	13	3.1	$4.3x10^{-3}$	$8.7x10^{-4}$	0.036
2020-12-09	10	2.3	$3.1x10^{-3}$	$6.8x10^{-4}$	0.040
2020-12-10	8.2	1.5	$1.8x10^{-3}$	$4.5x10^{-4}$	0.019
2020-12-11	5.5	0.82	$8.4x10^{-4}$	$2.2x10^{-4}$	0.010
2020-12-14	11	2.1	$2.6x10^{-3}$	$5.6x10^{-4}$	0.021
2020-12-17	7.1	1.4	$1.6x10^{-3}$	$3.7x10^{-4}$	0.016
2020-12-18	4.3	0.88	$1.1x10^{-3}$	$2.0x10^{-4}$	0.011
2020-12-21	7.9	2.8	$4.1x10^{-3}$	$8.3x10^{-4}$	0.038
2020-12-22	7.9	1.8	$2.6x10^{-3}$	$5.8x10^{-4}$	0.030
2020-12-24	3.0	0.60	$7.1x10^{-4}$	$2.0x10^{-4}$	0.010
2020-12-25	8.2	1.8	$2.0x10^{-3}$	$5.8x10^{-4}$	0.025
2020-12-26	5.7	1.6	$1.7x10^{-3}$	$4.5x10^{-4}$	0.023
2020-12-29	4.2	0.89	$8.8x10^{-4}$	$2.7x10^{-4}$	0.013
2020-12-30	12	2.6	$2.7x10^{-3}$	$7.8x10^{-4}$	0.039
2020-12-31	9.1	2.0	$2.0x10^{-3}$	$5.6x10^{-4}$	0.031
2021-01-01	14	2.8	$2.6x10^{-3}$	$8.0x10^{-4}$	0.050
2021-01-02	10	2.3	$2.3x10^{-3}$	$7.0x10^{-4}$	0.038
2021-01-03	13	2.7	$2.5x10^{-3}$	$7.4x10^{-4}$	0.030
2021-01-04	8.5	1.4	$1.4x10^{-3}$	$4.0x10^{-4}$	0.019
2021-01-05	6.2	0.73	$7.4x10^{-4}$	$2.7x10^{-4}$	0.013
2021-01-06	13	0.87	$6.5x10^{-4}$	$3.1x10^{-4}$	0.013
2021-01-07	14	1.4	$1.0x10^{-3}$	$4.4x10^{-4}$	0.015
2021-01-08	7.3	0.83	$5.8x10^{-4}$	$3.3x10^{-4}$	0.018
2021-01-10	8.0	0.82	$7.2x10^{-4}$	$2.8x10^{-4}$	0.011
2021-01-11	10	1.6	$9.3x10^{-4}$	$5.4x10^{-4}$	0.028

The mean emission rates of NH_3, MMA, DMA and TMA are listed in Table 3.3 together with literature values.

Table 3.3: The mean emission rates of NH_3 and the methylamines in g animal^{-1} h^{-1}.

Compound		Emission rate (g animal^{-1} h^{-1})§	
	This study	Literature values	
NH_3	1.5 ± 0.57	1.8 ± 1.3	(Kammer et al., 2020)
		0.67 - 1.10	(Janke et al., 2020)
		0.75 - 1.25	(Schmithausen et al. 2018)
		0.85 - 0.88	(Wang et al., 2016)
		0.64 ± 0.32	(Ngwabie et al., 2014)
		0.45 – 0.51	(Harper et al., 2009)
MMA	$1.9 \pm 0.9 \times 10^{-3}$		
DMA	$4.9 \pm 1.7 \times 10^{-4}$		
TMA	0.022 ± 0.011	0.020 ± 0.016	(Kammer et al.,2020)

§: Note that in the literature emissions rates are usually reported per livestock unit (LU), with a dairy cow corresponding to 1 LU. Since the weight and age of cattle in this study was not known, emission rates are reported per animal.

The mean NH_3 emission rate is on the higher end of the reported literature values. It must also be noted that in my study the ACR was measured, while it was derived from CO_2 mass balance in most of the cited studies. The measured ACR value is considered to me more accurate than the derived value.

The average TMA emission rate of 0.022 g animal^{-1} h^{-1} is in excellent agreement with the only value found in the literature. To the best of my knowledge, this is the first time that MMA or DMA emission rates from cattle have been determined.

The VMRs of NH_3 and MMA in the barn exhibited a pronounced increase with temperature (Fig. 3.5). Since the ACR did not exhibit a temperature dependence, this translates into a temperature-dependent increase of the NH_3 and MMA emission rates (Fig. 3.6). While the correlation between the two parameters is weak, the trend of a temperature-driven increase of emissions is still evident. The increase is less apparent for the emission rates of DMA and TMA (R^2 = 0.13 and 0.13, respectively) (Figs. 6.9 – 6.10). Since temperature data was only available for a limited number of days during the campaign, future work should cover a wider temperature range to better characterize the temperature dependence of NH_3 and amine emissions.

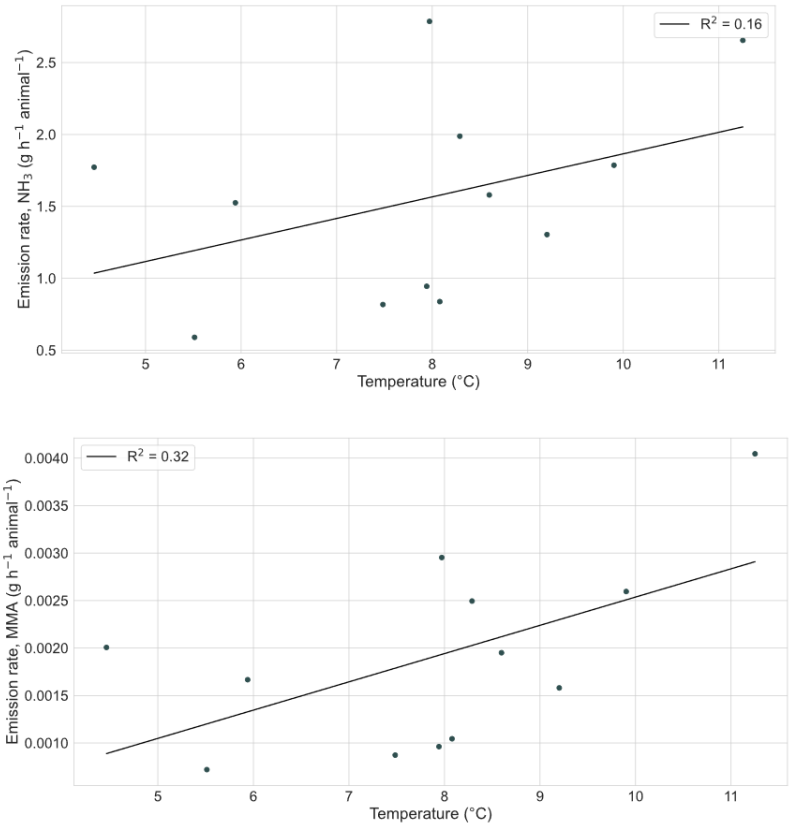

Figure 3.6: Emission rates (g animal^{-1} h^{1}) of NH_3 and MMA plotted as a function of air temperature in the barn.

3.2 Laboratory measurements at UiO

The results from the field measurements are difficult to interpret because the sources of amines in a barn can be manifold (e.g., excrements, breath, food, other materials used in the barn). A series of samples in the barn at SHF were thus collected and analyzed in the laboratory at UiO. At the time of the measurement, the PTR-ToF-MS instrument suffered from a high NH_4^+ and O_2^+ background, so that only DMA and TMA are reported. Figs. 3.7 and 3.8 show the signals of TMA and DMA, respectively, as recorded in the dynamic headspace of i) silage food, ii) manure collected from the floor of the cattle barn, iii) feces directly collected form the rectum of an animal, iv) food pellets and v) sawdust. The highest TMA signal was recorded from the headspace of feces, while manure emitted TMA to a much smaller extent. Interestingly, considerable amounts of TMA were also detected in the headspace of silage food, which consisted of fermented hay. This could be an additional source of TMA, which was implied

from the results of the field measurements. DMA was detected in the headspace of fresh manure and silage food. In the case of the latter, it was, however, only an initial burst with the signal rapidly dropping to zero. This suggests that DMA had accumulated in the headspace of the sampling vial during storage and that it was not produced in significant amounts at the time of the measurement.

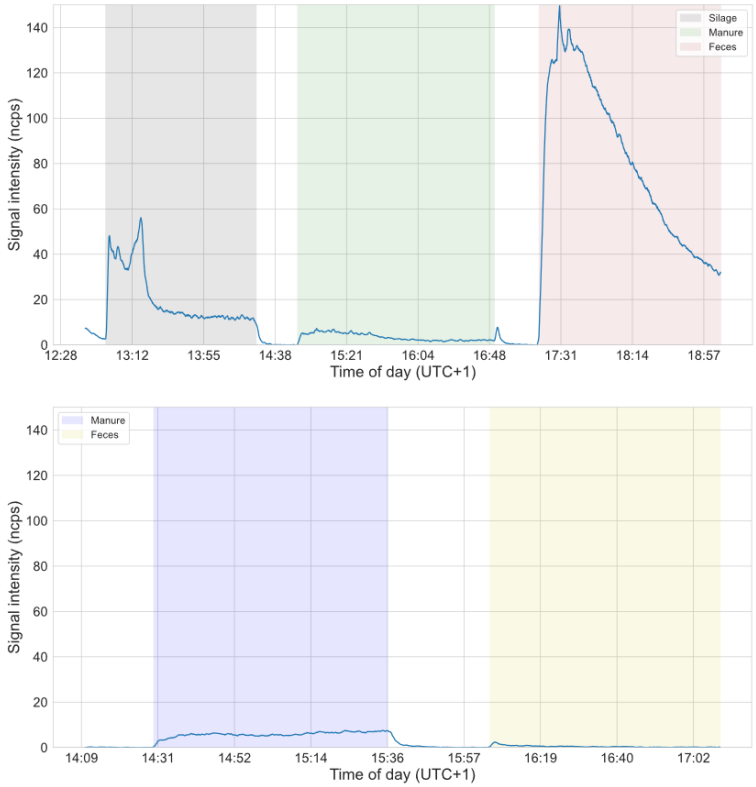

Figure 3.7: The signal (ncps) of TMA as recorded in the dynamic headspace of samples collected in the SHF barn. The samples include: i) silage food (fermented hay), ii) manure collected from the floor of the cattle barn, iii) feces directly collected form the rectum of an animal, iv) food pellets and v) sawdust.

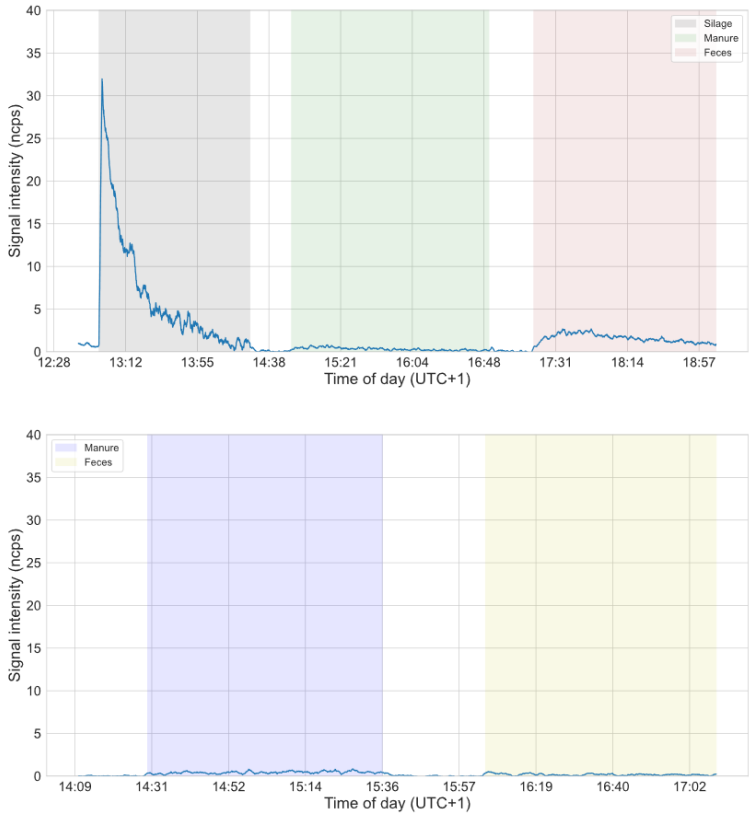

Figure 3.8: Same as Fig. 3.7 but for DMA.

4. Conclusion

In the cattle barn at SHF, TMA was the most abundant methylamine emitted with an emission rate of 22 ± 11 mg h^{-1} $animal^{-1}$, followed by MMA with an emission rate of 1.9 ± 0.9 mg h^{-1} $animal^{-1}$, and finally DMA with an emission rate of 0.49 ± 0.17 mg h^{-1} $animal^{-1}$. The emission rate of NH_3 was 1.5 ± 0.6 g h^{-1} $animal^{-1}$. Relative to NH_3, the abundance of MMA, DMA, and TMA were 0.78 x 10^{-3}, 0.11 x 10^{-3} and 4.6 x 10^{-3}, respectively. Mean emission rates of NH_3 and TMA were in accordance with previous work; However, they were in the higher end of the reported range for NH_3. According to the diurnal profiles, the methylamines exhibited a temperature dependence, an observation which was further suggested by plotting NH_3 and the methylamines as a function of the temperature. The temperature dependence was strongest for NH_3 and MMA. Since the ACR is independent of the temperature, the emission rates were also found to be temperature dependent, in particular NH_3 and MMA. More research is required to characterize the temperature dependence of NH_3 and the methylamines.

Linear regression analyses between NH_3 and the methylamines demonstrated a high level of correlation between NH_3, MMA, and DMA, which indicates that they originate from the same source, animal excrements being the most prominent candidate. The correlation between NH_3 and TMA was poorer, indicating some differences in formation and/or volatilization. To investigate additional sources, a linear regression was fitted between TMA and CH_4; however, no correlation was observed, and TMA is most likely not emitted from rumination. Laboratory measurements from UiO confirmed cattle feces as a prominent source of TMA; However, an additional, minor source was suggested: silage food. DMA was also detected in the headspace of silage food; However, it had most likely accumulated during storage and is thus not labeled as a significant source. More research is required to investigate this possible source of amines from cattle husbandry.

Even though cattle are typically characterized as the largest emitter of amines from animal husbandry, the contribution from other farm animals is not negligible. Future research should thus include field measurements on sheep, pigs, and poultry. Kammer et al. (2020) quantified larger TMA VMRs in a sheep pen than dairy barn. Furthermore, Schade & Crutzen (1995) found significant emissions of amines from both swine and horses, and VMRs of ~30 ppmV in a poultry pen, thus approximately one order of magnitude larger than the mean NH_3 VMRs obtained from SHF.

5. References

Almeida, J., Schobesberger, S., Kürten, A., Ortega, I. K., Kupiainen-Määttä, O., Praplan, A. P., Adamov, A., Amorim, A., Bianchi, F., Breitenlechner, M., David, A., Dommen, J., Donahue, N. M., Downard, A., Dunne, E., Duplissy, J., Ehrhart, S., Flagan, R. C., Franchin, A., Guida, R., Hakala, J., Hansel, A., Heinritzi, M., Henschel, H., Jokinen, T., Junninen, H., Kajos, M., Kangasluoma, J., Keskinen, H., Kupc, A., Kurtén, T., Kvashin, A. N., Laaksonen, A., Lehtipalo, K., Leiminger, M., Leppä, J., Loukonen, V., Makhmutov, V., Mathot, S., McGrath, M. J., Nieminen, T., Olenius, T., Onnela, A., Petäjä, T., Riccobono, F., Riipinen, I., Rissanen, M., Rondo, L., Ruuskanen, T., Santos, F. D., Sarnela, N., Schallhart, S., Schnitzhofer, R., Seinfeld, J. H., Simon, M., Sipilä, M., Stozhkov, Y., Stratmann, F., Tomé, A., Tröstl, J., Tsagkogeorgas, G., Vaattovaara, P., Viisanen, Y., Virtanen, A., Vrtala, A., Wagner, P. E., Weingartner, E., Wex, H., Williamson, C., Wimmer, D., Ye, P., Yli-Juuti, T., Carslaw, K. S., Kulmala, M., Curtius, J., Baltensperger, U., Worsnop, D. R., Vehkamäki, H., & Kirkby, J. (2013). Molecular understanding of sulphuric acid–amine particle nucleation in the atmosphere. *Nature, 502*(7471), 359-363. https://doi.org/10.1038/nature12663

Boguski, T. K. (2006). *Understanding Units of Measurement*. Retrieved March 28th, 2021 from https://cfpub.epa.gov/ncer_abstracts/index.cfm/fuseaction/display.files/fileid/14285

Domingo, N. G. G., Balasubramanian, S., Thakrar, S. K., Clark, M. A., Adams, P. J., Marshall, J. D., Muller, N. Z., Pandis, S. N., Polasky, S., Robinson, A. L., Tessum, C. W., Tilman, D., Tschofen, P., & Hill, J. D. (2021). Air quality–related health damages of food. *Proceedings of the National Academy of Sciences, 118*(20). https://doi.org/10.1073/pnas.2013637118

Ellis, A. M., & Mayhew, C. A. (2014). *Proton Transfer Reaction Mass Spectrometry - Principles and Applications*. John Wiley & Sons, Ltd. https://doi.org/10.1002/9781118682883

Ge, X., Wexler, A. S., & Clegg, S. L. (2011a). Atmospheric amines – Part I. A review. *Atmospheric Environment, 45*(3), 524-546. https://doi.org/10.1016/j.atmosenv.2010.10.012

Ge, X., Wexler, A. S., & Clegg, S. L. (2011b). Atmospheric amines – Part II. Thermodynamic properties and gas/particle partitioning. *Atmospheric Environment, 45*(3), 561-577. https://doi.org/10.1016/j.atmosenv.2010.10.013

Groot Koerkamp, P. W. G., Metz, J. H. M., Uenk, G. H., Phillips, V. R., Holden, M. R., Sneath, R. W., Short, J. L., White, R. P. P., Hartung, J., Seedorf, J., Schröder, M., Linkert, K. H., Pedersen, S., Takai, H., Johnsen, J. O., & Wathes, C. M. (1998). Concentrations and Emissions of Ammonia in Livestock Buildings in Northern Europe. *Journal of Agricultural Engineering Research, 70*(1), 79-95. https://doi.org/10.1006/jaer.1998.0275

Gross, J. H. (2017). *Mass Spectrometry - A Textbook* (Third ed.). Springer Berlin Heidelberg. https://doi.org/10.1007/978-3-642-10711-5

Harper, L. A., Flesch, T. K., Powell, J. M., Coblentz, W. K., Jokela, W. E., & Martin, N. P. (2009). Ammonia emissions from dairy production in Wisconsin1. *Journal of Dairy Science, 92*(5), 2326-2337. https://doi.org/10.3168/jds.2008-1753

Hunter, E. P. L., & Lias, S. G. (2017). Proton Affinities Determined Using Mass Spectrometry. In J. C. Lindon, G. E. Tranter, & D. W. Koppenaal (Eds.), *Encyclopedia of Spectroscopy and Spectrometry (Third Edition)* (pp. 779-784). Academic Press. https://doi.org/10.1016/B978-0-12-803224-4.00259-4

IONICON. (2021). *Liquid Calibration Unit* Retrieved Feb. 9th, 2021 from https://www.ionicon.com/accessories/details/liquid-calibration-unit-lcu

Ishler, V. A. (2016). Nitrogen, Ammonia Emissions and the Dairy Cow. Retrieved March 14th 2021, from https://extension.psu.edu/nitrogen-ammonia-emissions-and-the-dairy-cow

Janke, D., Willink, D., Ammon, C., Hempel, S., Schrade, S., Demeyer, P., Hartung, E., Amon, B., Ogink, N., & Amon, T. (2020). Calculation of ventilation rates and ammonia emissions: Comparison of sampling strategies for a naturally ventilated dairy barn. *Biosystems Engineering, 198*, 15-30. https://doi.org/10.1016/j.biosystemseng.2020.07.011

Kammer, J., Décuq, C., Baisnée, D., Ciuraru, R., Lafouge, F., Buysse, P., Bsaibes, S., Henderson, B., Cristescu, S. M., Benabdallah, R., Chandra, V., Durand, B., Fanucci, O., Petit, J.-E., Truong, F., Bonnaire, N., Sarda-Estève, R., Gros, V., & Loubet, B. (2020). Characterization of particulate and gaseous pollutants from a French dairy and sheep farm. *Science of The Total Environment, 712*. https://doi.org/10.1016/j.scitotenv.2019.135598

Kuhn, U., Sintermann, J., Spirig, C., Jocher, M., Ammann, C., & Neftel, A. (2011). Basic biogenic aerosol precursors: Agricultural source attribution of volatile amines revised. *Geophysical Research Letters, 38*(16). https://doi.org/10.1029/2011GL047958

Laussmann, D., & Helm, D. (2011). Air Change Measurements Using Tracer Gases: Methods and Results. Significance of air change for indoor air quality. https://www.intechopen.com/books/chemistry-emission-control-radioactive-pollution-and-indoor-air-quality/air-change-measurements-using-tracer-gases-methods-and-results-significance-of-air-change-for-indoor

Lee, D., & Wexler, A. S. (2013). Atmospheric amines – Part III: Photochemistry and toxicity. *Atmospheric Environment, 71*, 95-103. https://doi.org/10.1016/j.atmosenv.2013.01.058

Murphy, S. M., Sorooshian, A., Kroll, J. H., Ng, N. L., Chhabra, P., Tong, C., Surratt, J. D., Knipping, E., Flagan, R. C., & Seinfeld, J. H. (2007). Secondary aerosol formation from atmospheric reactions of aliphatic amines. *Atmos. Chem. Phys.*, *7*(9), 2313-2337. https://doi.org/10.5194/acp-7-2313-2007

Ngwabie, N. M., Jeppsson, K. H., Nimmermark, S., Swensson, C., & Gustafsson, G. (2009). Multi-location measurements of greenhouse gases and emission rates of methane and ammonia from a naturally-ventilated barn for dairy cows. *Biosystems Engineering, 103*(1), 68-77. https://doi.org/10.1016/j.biosystemseng.2009.02.004

Ngwabie, N. M., Vanderzaag, A., Jayasundara, S., & Wagner-Riddle, C. (2014). Measurements of emission factors from a naturally ventilated commercial barn for dairy cows in a cold climate. *Biosystems Engineering, 127*, 103-114. https://doi.org/10.1016/j.biosystemseng.2014.08.016

Nielsen, C. J., Herrmann, H., & Weller, C. (2012). Atmospheric chemistry and environmental impact of the use of amines in carbon capture and storage (CCS). *Chemical Society Reviews, 41*(19), 6684-6704. https://doi.org/10.1039/C2CS35059A

NMBU. (2021). *Senter for husdyrforsøk*. Retrieved Feb. 9th, 2021 from https://www.nmbu.no/tjenester/sentre/shf

Qiu, C., & Zhang, R. (2013). Multiphase chemistry of atmospheric amines. *Physical Chemistry Chemical Physics, 15*(16), 5738-5752. https://doi.org/10.1039/C3CP43446J

Saha, C. K., Ammon, C., Berg, W., Loebsin, C., Fiedler, M., Brunsch, R., & von Bobrutzki, K. (2013). The effect of external wind speed and direction on sampling point concentrations, air change rate and emissions from a naturally ventilated dairy building. *Biosystems Engineering, 114*(3), 267-278. https://doi.org/10.1016/j.biosystemseng.2012.12.002

Schade, G. W., & Crutzen, P. J. (1995). Emission of aliphatic amines from animal husbandry and their reactions: Potential source of N2O and HCN. *Journal of Atmospheric Chemistry, 22*(3), 319-346. https://doi.org/10.1007/BF00696641

Schmithausen, A., Schiefler, I., Trimborn, M., Gerlach, K., Südekum, K.-H., Pries, M., & Buescher, W. (2018). Quantification of Methane and Ammonia Emissions in a Naturally Ventilated Barn by Using Defined Criteria to Calculate Emission Rates. *Animals, 8*, 75. https://doi.org/10.3390/ani8050075

Sintermann, J., Schallhart, S., Kajos, M., Jocher, M., Bracher, A., Münger, A., Johnson, D., Neftel, A., & Ruuskanen, T. (2014). Trimethylamine emissions in animal husbandry. *Biogeosciences, 11*(18), 5073-5085. https://doi.org/10.5194/bg-11-5073-2014

Sorooshian, A., Murphy, S. M., Hersey, S., Gates, H., Padro, L. T., Nenes, A., Brechtel, F. J., Jonsson, H., Flagan, R. C., & Seinfeld, J. H. (2008). Comprehensive airborne characterization of aerosol from a major bovine source. *Atmos. Chem. Phys., 8*(17), 5489-5520. https://doi.org/10.5194/acp-8-5489-2008

Tofwerk. (2021). *Vocus PTR-TOF Webinar: Fundamentals and Applications*. Retrieved Feb. 17, 2021 from https://www.tofwerk.com/vocus-ptr-tof-webinar/

Wang, X., Ndegwa, P. M., Joo, H., Neerackal, G. M., Harrison, J. H., Stöckle, C. O., & Liu, H. (2016). Reliable low-cost devices for monitoring ammonia concentrations and emissions in naturally ventilated dairy barns. *Environmental Pollution, 208*, 571-579. https://doi.org/10.1016/j.envpol.2015.10.031

Yu, F., & Luo, G. (2014). Modeling of gaseous methylamines in the global atmosphere: impacts of oxidation and aerosol uptake. *Atmos. Chem. Phys., 14*(22), 12455-12464. https://doi.org/10.5194/acp-14-12455-2014

6. Appendix

6.1 Formulas, calculations, and sample preparation

The conversion of concentrations (mol/L) into VMRs (ppbV) when using the LCU. The formula was provided by IONICON, who constructed the LCU:

$$\text{VMR (ppbV)} = \text{LCU Liquid Flow (µL/min)} * \frac{\text{Molar volume ideal gas (L/mol)}}{\text{LCU standard gas flow (µL/min)}} * C_{solution}\ \text{(mol/L)} * 10^9 \quad (6.1)$$

The calculation of the amount of analyte in $g_{analyte}/L_{solvent}$ to make calibration solutions (based on Eq. 6.1) :

$$g_{analyte}/L_{solvent} = \frac{\text{VMR (ppbV)}}{\text{LCU liquid flow (µL/min)}} * \frac{\text{LCU standard gas flow (µL/min)}}{\text{Molar volume of ideal gas (L/mol)}} * MW_{analyte}\ \text{(g/mol)} * 10^{-9} \quad (6.2)$$

The conversion of $g_{analyte}/L_{solvent}$ to $mL_{analyte}/L_{solvent}$:

$$mL_{analyte}/L_{solvent} = \frac{g_{analyte}/L_{solvent}}{\rho_{analyte}(g/mL)} \quad (6.3)$$

where $\rho_{analyte}$ = the density of the analyte (g/mL).

Calculations for the sample preparation of NH_3, MMA, DMA, and TMA solutions for the LCU-calibrations. All solutions were diluted by HPLC-water:

Solution of 10 ppmV NH_3 at 10 µL/min LCU liquid flow and 1 L/min dilution flow:

$$g_{NH3}/L = \frac{12000\ ppbV}{10\ \mu L/min} * \frac{10^6 \mu L/min}{22.4\ L} \quad (6.4a)$$

$$* \ 17.02655\ g/mol * 10^{-9} = 0.912\ g/L$$

$$mL_{NH3}/L = \frac{0.912\ g_{NH3}/L_{solvent}}{0.900\ g/mL} = 1.01\ mL/L \quad (6.4b)$$

The density of pure NH_3 is 0.00073 g/mL; however, the NH_3 density in the diluted stock solution (with 28 % NH_3) was approximately equal to the density of the solvent (H_2O).

Stock solution from manufacturer contained 28 % NH_3:

$$\frac{1.01\ mL/L}{0.28} = 3.72\ mL/L \quad (6.4c)$$

Solution of 10 ppmV MMA at 10 µL/min LCU liquid flow and 1 L/min dilution flow:

$$g_{MMA}/L = \frac{10000\ ppbV}{10\ \mu L/min} * \frac{10^6 \mu L/min}{22.4\ L} \quad (6.5a)$$

$$* \ 31.0422\ g/mol * 10^{-9} = 1.39\ g/L$$

$$mL_{MMA}/L = \frac{1.39\ g_{MMA}/L_{solvent}}{0.700\ g/mL} = 1.98\ mL/L \quad (6.5b)$$

Stock solution for manufacturer contained 40 % MMA:

$$\frac{1.98\ mL/L}{0.40} = 4.95\ mL/L \quad (6.5c)$$

Solution of 10 ppmV DMA at 10 µL/min LCU liquid flow and 1 L/min dilution flow:

$$g_{DMA}/L = \frac{10000\ ppbV}{10\ \mu L/min} * \frac{10^6 \mu L/min}{22.4\ L} \quad (6.6a)$$

$$* \ 45.0579\ g/mol * 10^{-9} = 2.01\ g/L$$

$$mL_{DMA}/L = \frac{2.01\ g_{DMA}/L_{solvent}}{0.670\ g/mL} = 3.00\ mL/L \quad (6.6b)$$

Stock solution from manufacturer contained 40 % DMA:

$$\frac{3.00\ mL/L}{0.40} = 7.51\ mL/L \quad (6.6c)$$

Solution of 10 ppmV TMA at 10 µL/min LCU liquid flow and 1 L/min dilution flow:

$$g_{TMA}/L = \frac{10000\ ppbV}{10\ \mu L/min} * \frac{10^6 \mu L/min}{22.4\ L} \quad (6.7a)$$

$$* \ 59{,}0735\ g/mol * 10^{-9} = 2.64\ g/L$$

$$mL_{TMA}/L = \frac{2.64\ g_{TMA}/L_{solvent}}{0.670\ g/mL} = 3.94\ mL/L \quad (6.7b)$$

Stock solution from manufacturer contained 45 % TMA: (6.7c)

$$\frac{3.94\ mL/L}{0.45} = 8.75\ mL/L$$

Finally, all solutions prepared according to Eq. 6.4a – 6.7c were diluted from volume mixing ratios of 10 ppmV to 10 ppbV. Thus, 1 mL was extracted from the respective 10 ppmV solution and diluted with 1000 mL HPLC-water in a 1 L Erlenmeyer flask:

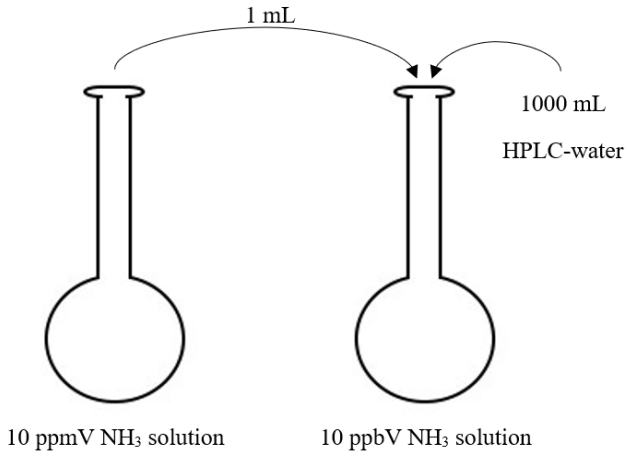

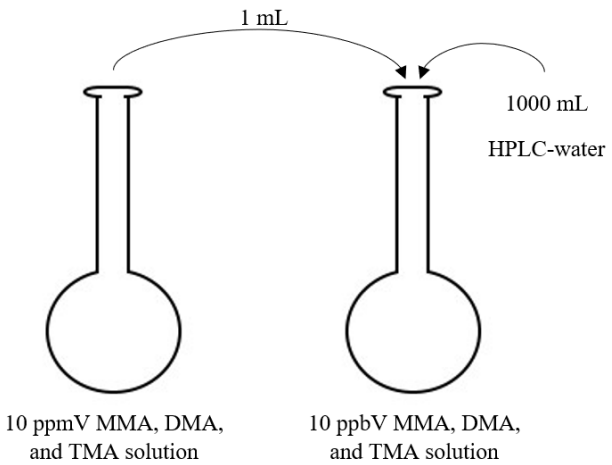

6.2 Figures

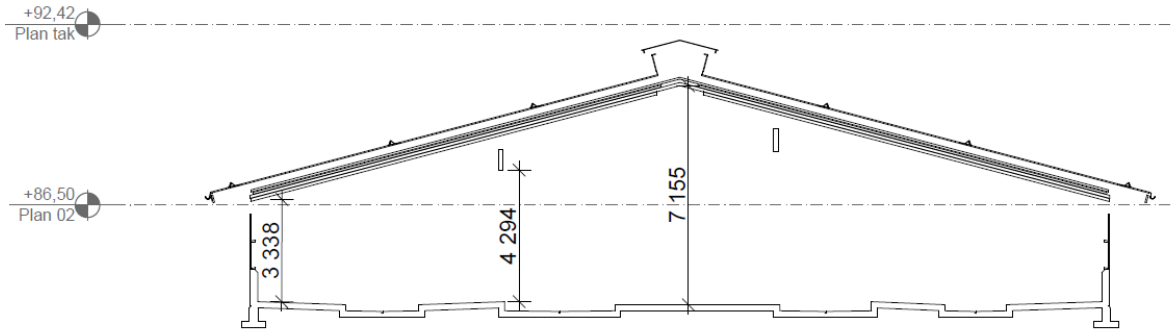

Figure 6.1: Schematics of the height (in mm) of the cattle barn, used for the calculation of a room volume.

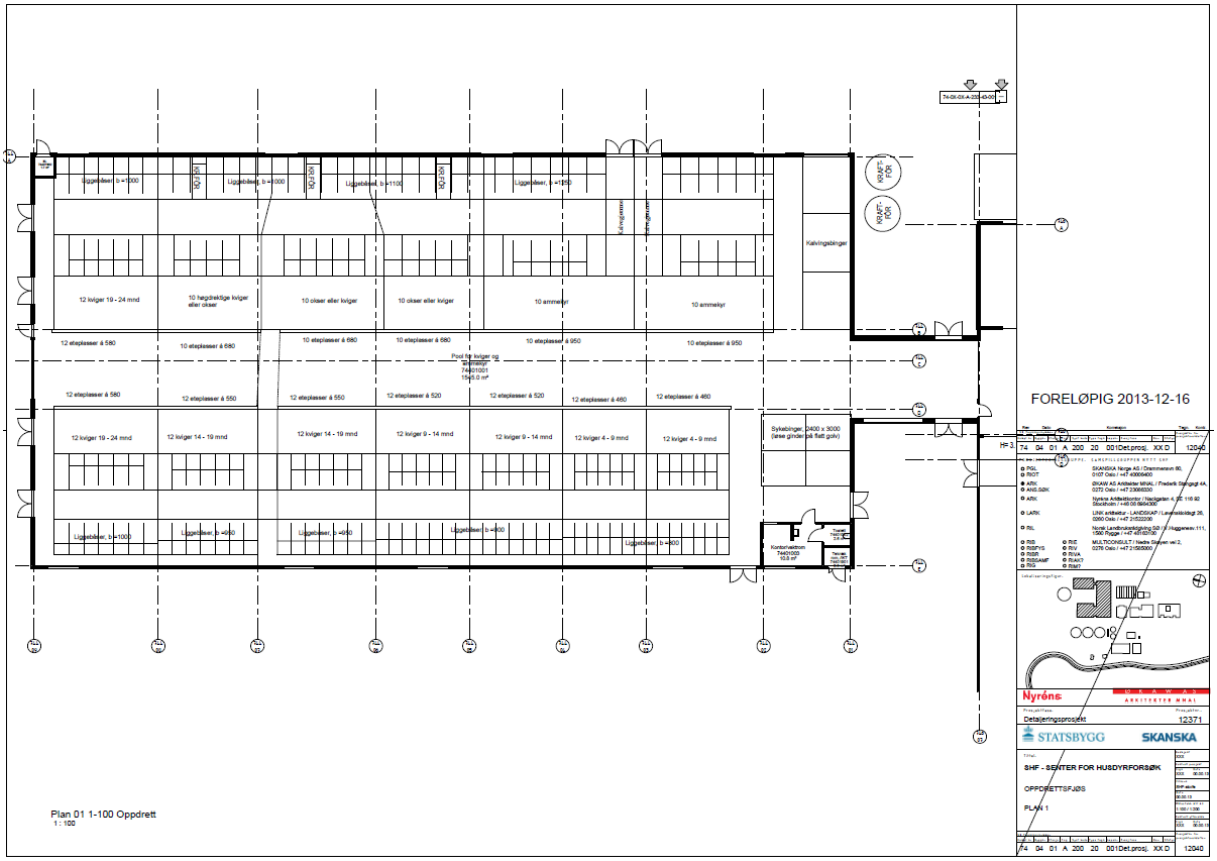

Figure 6.2: Schematics of the inside of the cattle barn, used for the calculation of a room volume. The area of the barn is specified in this figure: 1545 m^2.

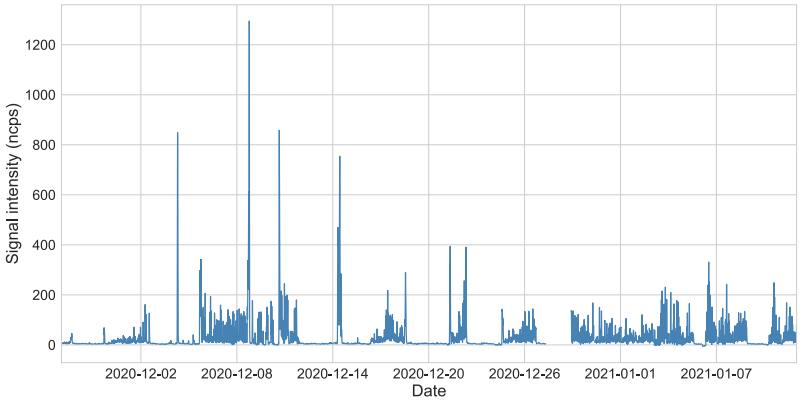

Figure 6.3: The time series of methanethiol (ncps) as a 30-minute moving-average.

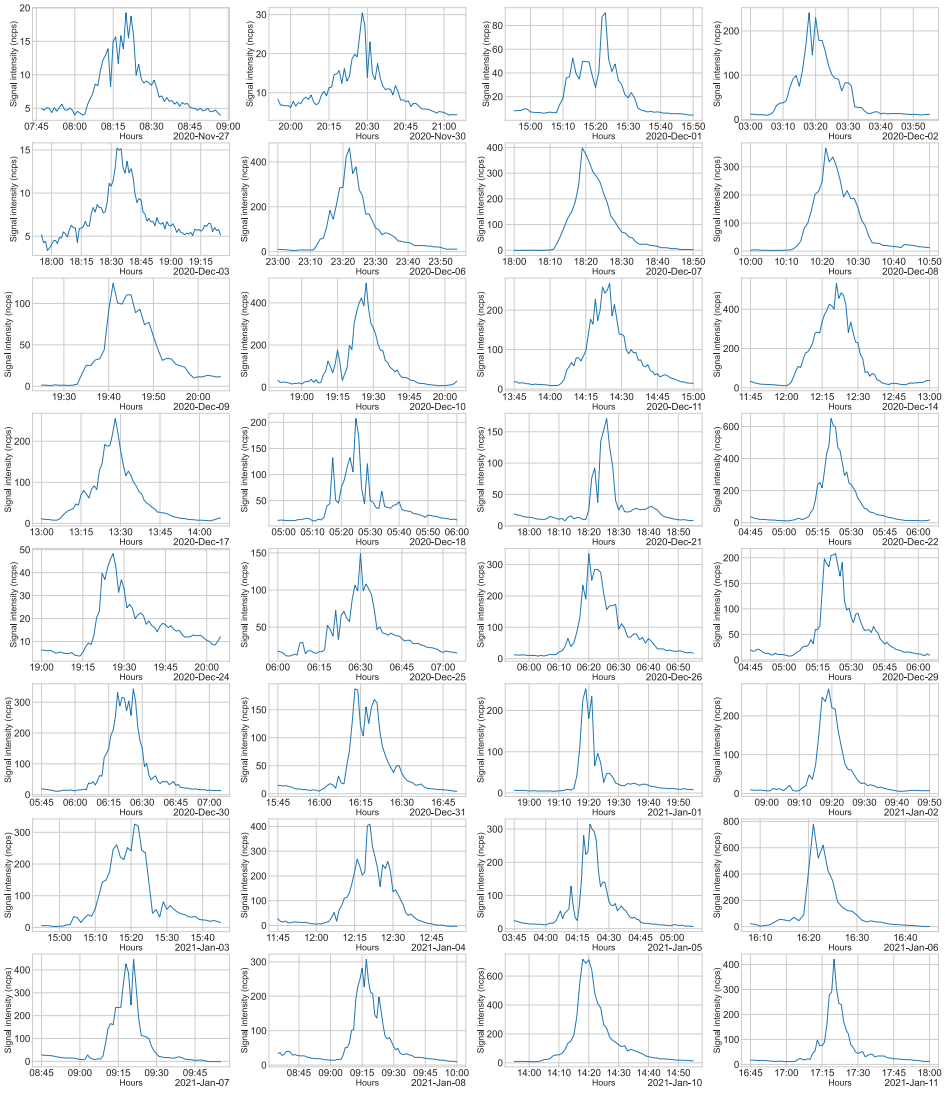

Figure 6.4: The peaks of methanethiol (ncps) selected for the calculation of the ACR, plotted in a linear scale.

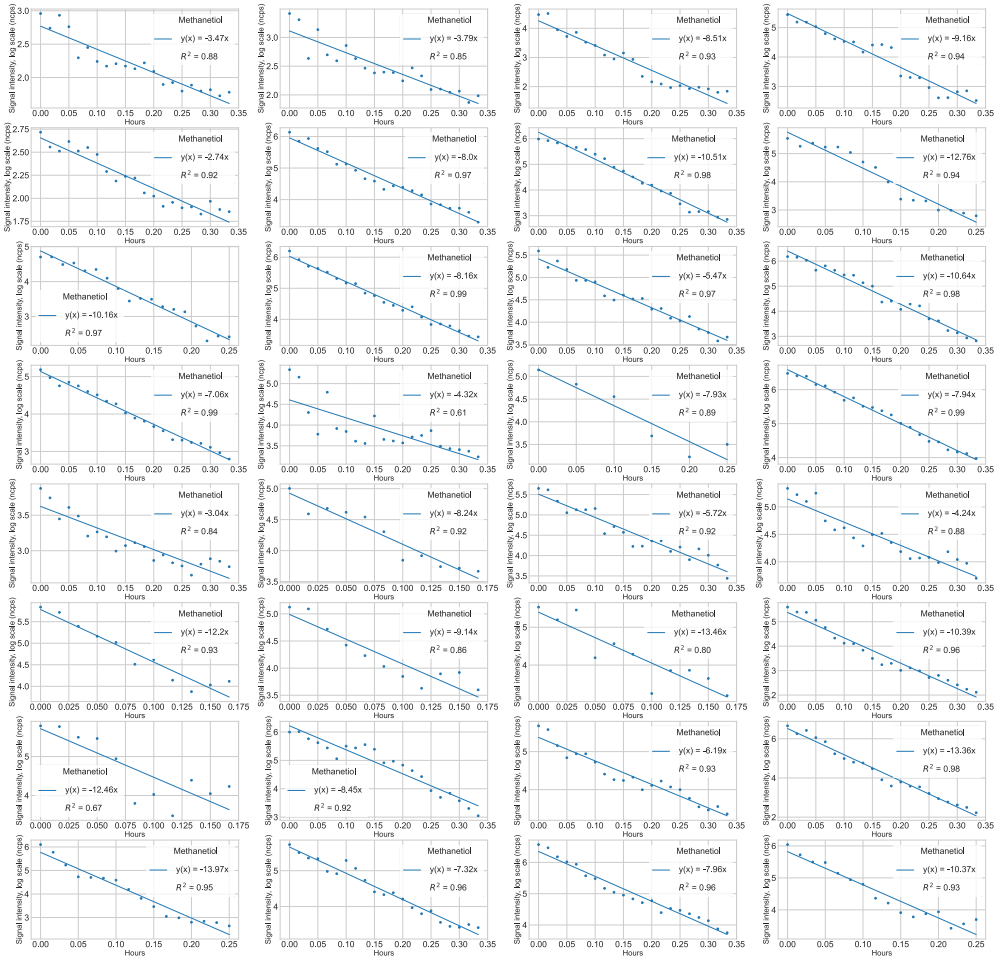

Figure 6.5: Linear regression of the methanethiol decay rates for the selected peaks presented in Fig. 6.4, plotted in a logarithmic scale. The dates are not specified; however, the set-up is corresponding to the dates and timestamps in Fig. 6.4.

Figure 6.6: Samples collected from a cattle barn at SHF. From left: Food pellets, silage, sawdust, “old” manure, and “fresh” manure.

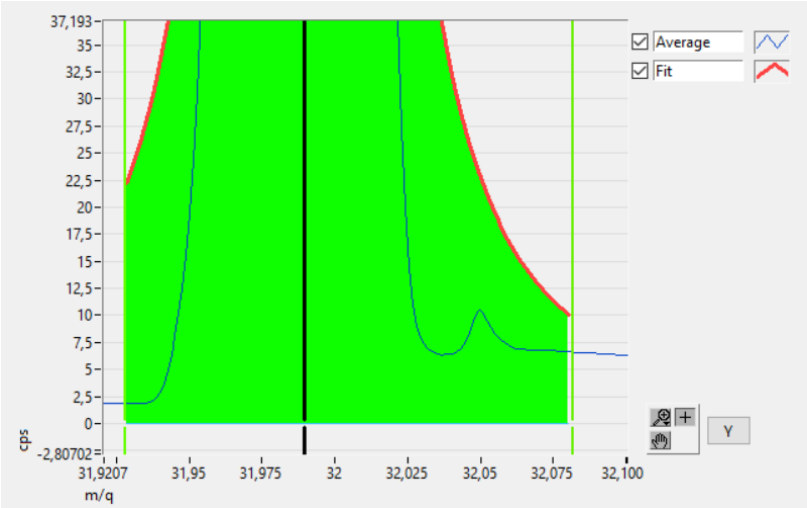

Figure 6.7: The peaks assigned to O_2^+ (green), and MMA (small peak at *m/z* 32.05) from the measurements on samples from a cattle barn at SHF. The signal of O_2^+ was intense, thus, MMA was not integrated in the mass spectrum.

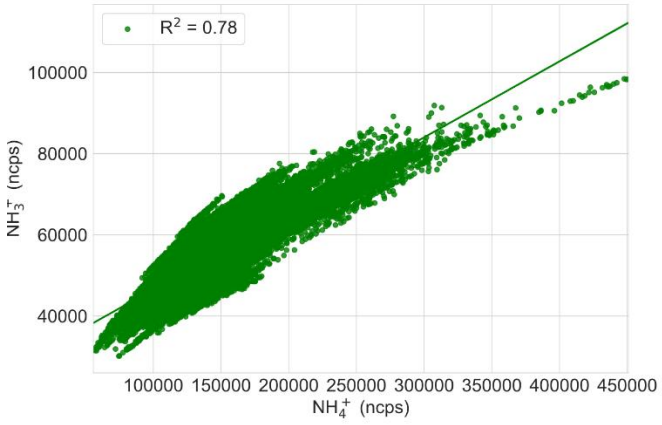

Figure 6.8: Linear regression between the raw data (cps) of NH_3^+ at accurate *m/z* 17.025 (y-axis) and NH_4^+ at accurate *m/z* 18.034 (x-axis).

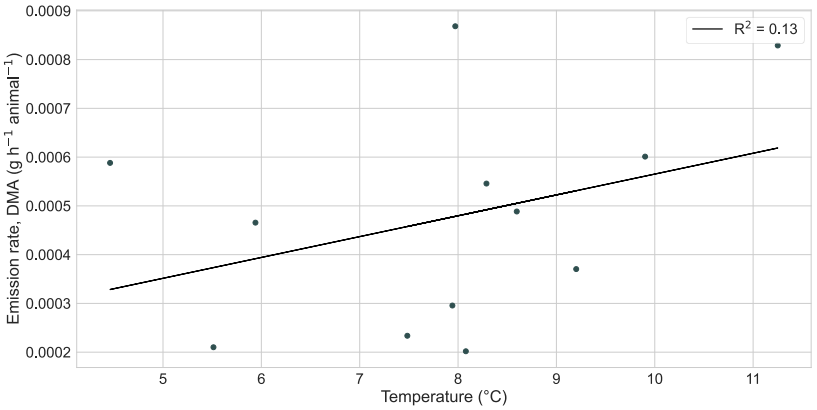

Figure 6.9: Emission rates (g animal^{-1} h^{1}) of DMA plotted as a function of air temperature in the barn.

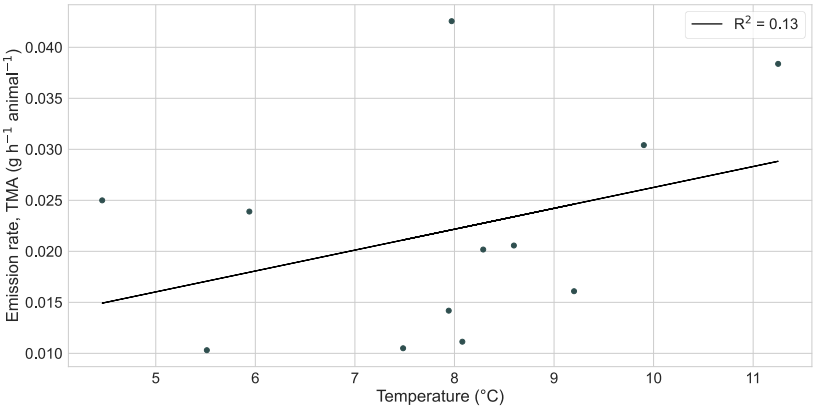

Figure 6.10: Same as Fig. 6.9 but for TMA.